EXAMINING TEMPORAL VARIATIONS OF PHYTOPLANKTON PHOTOACCLIMATION USING A NOVEL FLUORESCENCE BASED APPROACH

by

Adam J. Comeau

Submitted in partial fulfillment of the requirements
for the degree of Master of Science

at

Dalhousie University
Halifax, Nova Scotia
August 2010

DALHOUSIE UNIVERSITY

DEPARTMENT OF OCEANOGRAPHY

The undersigned hereby certify that they have read and recommend to the Faculty of Graduate Studies for acceptance a thesis entitled “EXAMINING TEMPORAL VARIATIONS OF PHYTOPLANKTON PHOTOACCLIMATION USING A NOVEL FLUORESCENCE BASED APPROACH” by Adam J. Comeau in partial fulfillment of the requirements for the degree of Master of Science.

Dated: August 20, 2010

Supervisor:_____

Readers:_____

_____

_____

Graduate Coordinator:_____

DALHOUSIE UNIVERSITY

Date: August 20, 2010

AUTHOR: Adam J. Comeau

TITLE: EXAMINING TEMPORAL VARIATIONS OF PHYTOPLANKTON PHOTOACCLIMATION USING A NOVEL FLUORESCENCE BASED APPROACH

DEPARTMENT OR SCHOOL: Department of Oceanography

DEGREE: MSc CONVOCATION: October YEAR: 2010

“We may not know exactly what we are measuring, but the patterns observed are too strong to ignore.” (Cullen and Renger, 1979)

Table of Contents

List of Tables

List of Figures

Abstract

Models of primary production require parameters to describe photosynthesis as a function of irradiance, such as the saturation irradiance (E_k, μmol photons m^{-2} s^{-1}). However, this parameter varies in both time and space, is expensive to measure, and its variability in the oceans is not well described. A novel fluorescence-based approach is presented to determine an empirical parameter (E_{FT}, μmol photons m^{-2} s^{-1}), which is strongly correlated with E_k. This correlation provides evidence to use E_{FT} as a proxy for E_k. Using an autonomous profiling instrument package (SeaHorse™, located on the Scotian Shelf) and an autonomous oceanographic observational buoy (Land/Ocean Biogeochemical Observatory, located in the Northwest Arm, N.S., Canada), the variability of E_{FT} was examined on three time scales: hours, days, and seasons. Studying variations of E_{FT} with these autonomous instruments provided insights to its variability on time scales relevant to models of primary production.

List of Abbreviations and Symbols Used

General oceanography

Chl*a*	Concentration of chlorophyll *a*	mg Chl*a* m^{-3}
$\overline{Chl_\ell}$	Concentration of chlorophyll *a* averaged throughout the mixed layer	mg Chl*a* m^{-3}
$P_{Z,T}$	Daily primary production of the water column	mg C m^{-2}
CTD	An instrument that measures conductivity, temperature, and depth, often attached to a package that also contains an *in vivo* fluorometer	
LOBO	Land/Ocean Biogeochemical Observatory (Satlantic, Inc.)	
ℓ	Depth of the surface mixed layer	m
w^*	Turbulent friction velocity	m s^{-1}
ρ_a	A typical air density, 1.2	kg m^{-3}
ρ_w	A typical water density, 1.025 x 10^{-3}	kg m^{-3}
C_{10}	Drag coefficient of 10 m wind speed on the sea surface 1.3 x 10^{-3}	unitless
U_{10}	Wind speed at 10 m above sea level	m s^{-1}
t_m	The mixing time scale of phytoplankton in the mixed layer	s
D	Day length	h^{-1}

Fluorescence

F vs. E	Fluorescence yield *vs.* irradiance	
rfu	Relative fluorescence units	
F	Fluorescence emitted per volume	µmol photons m^{-3} s^{-1}

F'	Fluorescence measured in the water column with an active fluorometer that flashes weak pulses of blue light, such as the common WET Labs ECO Pucks™	rfu
F'_N	Median nighttime F' between the hours of 0100 and 0400 (local time) for the LOBO data set	rfu
F'_{Ni}	A time series of F'_N interpolated throughout each day.	rfu
F'^*	*In vivo* fluorescence (F') normalized to nighttime fluorescence interpolated throughout the day $F'^* \equiv F' \cdot \left(F'_{Ni}\right)^{-1}$	unitless
ϕ_f	Quantum yield of fluorescence	photons fluoresced (photons absorbed)$^{-1}$
ϕ_{fo}	The quantum yield of fluorescence under no ambient light	photons fluoresced (photons absorbed)$^{-1}$
$\phi_{f\max}$	The maximum quantum yield of fluorescence of the Morrison (2003) model	photons fluoresced (photons absorbed)$^{-1}$
PAM	Pulse Amplitude Modulated fluorescence protocol	
m_1	The initial slope of the E.F.T. model	rfu
m_2	The second slope of the E.F.T. model	rfu
F'_{EFT}	The E.F.T. model estimate of fluorescence at the irradiance E_{FT}	rfu
E_{FT}	The threshold irradiance where F' begins to decrease as a function of irradiance	µmol photons m^{-2} s^{-1}
$E_{FT\text{-}pro}$	E_{FT} determined from a vertical profile	µmol photons m^{-2} s^{-1}
$E_{FT\text{-}moor}$	E_{FT} determined from a fixed depth time series	µmol photons m^{-2} s^{-1}
$E_{FT\text{-}pam}$	E_{FT} determined from a PAMotron, (see text)	µmol photons m^{-2} s^{-1}
z_{EFT}	The depth at which E_{FT} occurs	m

E_{fopt}	Irradiance at the maximum fluorescence of Morrison's (2003) model	µmol photons m^{-2} s^{-1}
qE	Energy dependent nonphotochemical quenching of fluorescence	unitless
qI	Inhibition quenching of fluorescence	unitless
qP	Photochemical quenching of fluorescence	
NPQ	Nonphotochemical quenching of fluorescence, a term that refers to both qE and qI	unitless
F_v / F_m	Photochemical efficiency of phytoplankton estimated from fluorescence	unitless
Q_a^*	Intracellular reabsorption factor for fluorescence	unitless
E.F.T.	Empirical Fluorescence Threshold	

Photosynthesis

P vs. E	Photosynthesis versus irradiance	
$P_{\max}^{Chla}$	Maximum rate of photosynthesis normalized to Chl*a*	mg C (mg Chl*a*)$^{-1}$ h^{-1}
E_k	Light saturation parameter of the *P vs. E* relationship	µmol photons m^{-2} s^{-1}
$\alpha^{\text{Chl}a}$	Initial slope of the *P vs. E* curve normalized to Chl*a*	mg C (mg Chl*a*)$^{-1}$ h^{-1} (µmol photons m^{-2} s^{-1})$^{-1}$
E_T	Threshold irradiance for photoinhibition	µmol photons m^{-2} s^{-1}

Light

PAR	Photosynthetically active radiation; 400 to 700 nm	µmol photons m^{-2} s^{-1}
E_o(PAR)	Scalar irradiance, in the PAR wavebands	µmol photons m^{-2} s^{-1}

$E_o(z,\mathrm{PAR})$	Scalar irradiance, in the PAR wavebands, at a depth z. The symbol z can be replaced by 0^+, 0^- or ℓ to represent just above, just below the sea surface, or at the base of the surface mixed layer	µmol photons m^{-2} s^{-1}
$\overline{E_o(\ell,PAR)}$	Average E_o(z,PAR) over the mixed layer	µmol photons m^{-2} s^{-1}
$E_o(0^-,\mathrm{PAR})_m$	Midday $E_o(0^-,\mathrm{PAR})$	µmol photons m^{-2} s^{-1}
$E_d(0^+,\mathrm{total})$	Downwelling irradiance above the sea surface measured over 285 nm to 2800 nm	W m^{-2}
$\overline{a^*_{phy}}$	Spectrally averaged chlorophyll *a* specific absorption coefficient weighted by the PAR wavebands (Babin *et al.,* 1996)	m^2 (mg Chl*a*)$^{-1}$
$K_o(\mathrm{PAR})$	Vertical diffuse scalar attenuation coefficient determined from near surface to the 1% light depth across the PAR wavebands	m^{-1}
$K_d(\ell,443)$	Vertical diffuse downwelling attenuation coefficient determined from 0 to ℓ measured at 443 nm	m^{-1}
τ_ℓ	Optical depth of the mixed layer	unitless
r	Non-dimensional reflection value	unitless

Acknowledgements

I would like to thank the entire plankton lab for their help and support. In particular, Arnaud Laurent, Chris Jones, Audrey Barnett, Susanne Craig, Richard Davis, Diego Ibarra, Cathy Ryan, Dave Bowen, Dave Ciochetto, and the ASX07 sampling volunteers, have helped me learn many aspects along the way: everything from practical field issues, data analysis, oceanography concepts, to MATLAB code. I would also like to thank Dr. Blair Greenan for providing access to the SeaHorse™ data set, Dr. Marlon Lewis for the LOBO data set, and Audrey Barnett for letting me use data from her thesis experiments. My supervising committee, Dr. Katja Fennel, and Dr. Keith Thompson, and external examiner, Dr. Mary Jane Perry helped me write a better thesis by providing insightful comments which allowed me to address problems from a different perspective.

It is needless to say I thank Dr. John Cullen. His insights and criticisms have helped me develop my critical thinking and writing skills. Among the many things he has taught me, two in particular stand out. 1) Never take measurements from an instrument for granted and always make sure it is measuring what you want it to measure. This seems a like basic skill, but I have developed a new appreciation it studying with Dr. Cullen. I am grateful for the opportunities he has provided for me.

A final special thanks to Myriam and Clarisse, the loves of my life. Thank you for your patience and support.

This research was supported by NSERC/Satlantic Industrial Research Chair in Environmental Observation Technology, NSERC Discovery Grants, the U.S. Office of Naval Research, and Canadian Foundation for Climate and Atmospheric Sciences.

Chapter 1: Introduction

Photosynthetic primary productivity is the rate of light-driven synthesis of organic matter from inorganic matter. In the ocean, phytoplankton are responsible for the bulk of the production and in this sense forms the basis of most marine food webs. Since photosynthetic primary production links inorganic and organic matter, it imposes fundamental constraints on biogeochemical processes. Many studies of pelagic food webs, carbon export to the deep sea and fisheries production utilize oceanic primary production (Iverson, 1990; Eppley and Peterson, 1979). Therefore there is a need for accurate and precise estimates of primary production for all regions of the ocean.

Local estimates of primary productivity, either from uptake of radioisotopic labeled bicarbonate or evolution of oxygen, have been made and improved upon for many decades (Marshall and Orr, 1928; Talling, 1957; and see overview by Barber and Hilting, 2002). Also, data sets from water samples have been compiled to describe patterns on a global scale (Koblentz-Mishke *et al*., 1970). However, this early method of estimating primary production on a global scale lacks adequate seasonal and spatial resolution due to the limited availability of data.

The deployment of the Coastal Zone Color Scanner (CZCS), carried aboard the Nimbus 7 satellite in 1978 (Longhurst *et al*., 1995), allowed for the first time high spatial and temporal resolution of estimates of sea surface concentrations of chlorophyll *a* throughout the oceans (Gordon *et al.,* 1980). Combined with estimates of sea surface incident irradiance (Bishop and Rossow, 1991), the information obtained from the CZCS was used with models to estimate primary production on a global scale (Platt, 1986). Since the CZCS, satellites with increased

sensor resolution (spectral and temporal), such as SeaWiFS and MODIS, have been deployed and primary production algorithms suitable for remote sensing applications continually improve (Platt and Sathyendranath, 1993; Antoine and Morel, 1996; Behrenfeld and Falkowski, 1997). Many models have been developed and comparisons between them have been made (Platt and Sathyendranath, 1993; Campbell *et al*., 2002; Carr *et al*., 2006). Models of primary production rely, either explicitly or implicitly, on assumed parameters of the photosynthesis versus irradiance (*P vs. E*) relationship (Fig. 1), such as the maximum rate normalized to chlorophyll *a* ($P_{\max}^{\mathrm{Chl}a}$, mg C (mg Chl*a*)$^{-1}$ h^{-1}) and the saturation irradiance (E_k, µmol photons m^{-2} s^{-1}) (Platt and Sathyendranath, 1993). Since satellites are not capable of directly estimating these parameters, which vary in both time and space (Côté and Platt, 1983; Harrison and Platt, 1986; Platt and Sathyendranath, 1993; Kyewalyanga *et al.,* 1998), assumptions are required to use them in models of primary productivity (Platt and Sathyendranath, 1993). In some models, the parameters that describe the *P vs. E* relationship have been assumed constant (Balch et al., 1992; Antoine and Morel, 1996), while others assume they vary according to empirical relationships (Antoine and Morel, 1996; Behrenfeld and Falkowski, 1997; but see Platt *et al*., (2008) for a new method where photosynthetic parameters are chosen from a large database based on similar environmental conditions, time, and location).

This thesis will examined a new method to estimate E_k, a key photosynthetic parameter, from two different autonomous oceanographic observing systems. This method can be applied equally to historical and new data sets to gather more information to improve the understanding of the temporal and spatial variability of E_k.

1.1 Parameters of the Photosynthesis *vs.* Irradiance Relationship

Photosynthetic parameters are used to describe the relationship between *P vs. E* (Fig. 1). At low irradiance, photosynthesis is limited by light, and therefore increases with increasing irradiance, as illustrated by the initial slope of the *P vs. E* curve ($\alpha^{\mathrm{Chl}a}$, mg C (mg Chl*a*)$^{-1}$ h^{-1} (µmol photons m^{-2} s^{-1})$^{-1}$). However, above the saturation irradiance, E_k (Talling, 1957), photosynthesis becomes light saturated and the maximum normalized rate of photosynthesis ($P_{\mathrm{max}}^{\mathrm{Chl}a}$) is approached (Sakshaug *et al*., 1997). Semi-empirical models have been developed and compared to explain the *P vs. E* relationship. The three parameters of the *P vs. E* relationship are related by $E_k = P_{\mathrm{max}}^{\mathrm{Chl}a} / \alpha^{\mathrm{Chl}a}$ and therefore only two parameters are required in the models (Talling, 1957; Jassby and Platt, 1976; Platt and Sathyendranath, 1993). Inhibition of photosynthesis in high irradiance can be described with an additional parameter (Platt *et al.,* 1980), but the process is not a first order influence on the estimation of productivity per unit area (Platt *et al.,* 1990) and will not be addressed in this thesis.

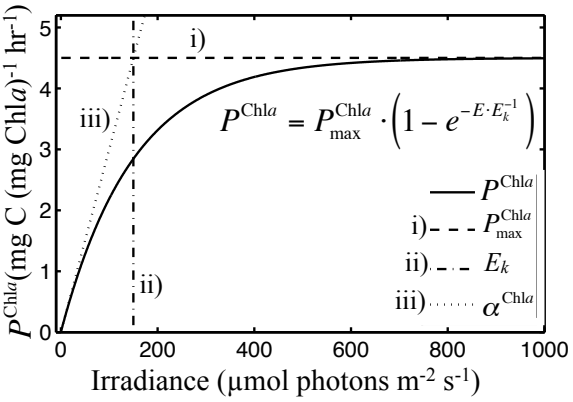

Figure 1. A generalized photosynthesis versus irradiance curve. The three parameters describing this curve are included: i) the maximum rate of photosynthesis normalized to chlorophyll *a* (P_{max}^{Chla}, mg C (mg Chla)$^{-1}$ h^{-1}) ii) the light saturation parameter (E_k, µmol photons m^{-2} s^{-1}), and iii) the initial slope of the *P vs. E* relationship (α^{Chla}, mg C (mg Chla)$^{-1}$ h^{-1} (µmol photons m^{-2} s^{-1})$^{-1}$). This relationship can be described with any two of these parameters.

The canonical form of a model that estimates daily primary production of the water column ($P_{Z,T}$, mg C m^{-2}) as a function of chlorophyll *a,* and light (Platt and Sathyendranath, 1993) shows how models of primary productivity depend on parameters of the *P vs. E* relationship:

$$P_{Z,T} = \frac{Chla \cdot P_{max}^{Chla} \cdot D}{K_o(PAR)} \cdot f\left(\frac{E_o(0^-, PAR)_m}{E_k}\right) \quad (1)$$

where Chl*a* is the concentration of chlorophyll (mg Chl*a* m^{-3}), D is day length (h^{-1}), $E_o(0^-,\mathrm{PAR})_m$ is the surface photosynthetically available radiation from 400-700 nm (PAR) just below the surface at midday (µmol photons m^{-2} s^{-1}), K_o(PAR) is the vertical diffuse scalar attenuation coefficient of PAR evaluated to the 1% light level (m^{-1}) (Kirk, 1994), P_{max}^{Chla} and E_k are the photosynthetic parameters mentioned above, and f is a dimensionless function that describes the cumulative influence of irradiance on water column photosynthesis as influenced by the *P vs. E* curve and surface irradiance. There are other ways to estimate $P_{Z,T}$, such as depth or spectrally resolved models (Platt *et al*., 1988; Sathyendranath and Platt, 1989; Behrenfeld and

Falkowski, 1997). However, Eq. (1) forms the basis of simple analytical models for estimating daily local estimates of primary production to yearly global estimates, and is sufficient to demonstrate the need for photosynthetic parameters of phytoplankton: $P_{\max}^{\mathrm{Chl}a}$ directly scales $P_{Z,T}$ and E_k specifies its dependence on surface irradiance. Since E_k is contained within the function "f" (Eq. 1) it does not scale $P_{Z,T}$ directly. However over a typical range of irradiance, a 50% underestimate of E_k will result in a ~30% overestimate of $P_{Z,T}$ (see Fig. A1 of Platt and Sathyendranath, 1993).

Photosynthetic parameters vary widely for a number of reasons including species composition (Côté and Platt, 1983; MacIntyre *et al*., 2002), nutritional status (Herzig and Falkowski, 1989; Cullen *et al.*, 1992b; Babin *et al*., 1996b; Barnett, 2005), and light history (Prézelin and Matlick, 1980; Lewis *et al*., 1984; MacIntyre *et al*., 2002; Barnett, 2005). It is therefore important to understand their variability to properly model primary production (Sakshaug *et al*., 1997). There are a number of studies that have examined the variability of $P_{\max}^{\mathrm{Chl}a}$ (Côté and Platt 1983; Harding *et al.,* 1982; Harrison and Platt, 1986, Shaw and Purdie, 2001; Goebel and Kremer, 2007); however this work focuses on E_k. Even though the variability of E_k has been related to surface irradiance (Behrenfeld and Falkowski, 1997) and average irradiance for the previous 3 days (Platt and Sathyendranath, 1993), other attempts at developing predictive models from environmental variables have had limited success (Coté and Platt, 1983; Shaw and Purdie, 2001; Goebel and Kremer, 2007).

1.2 Photoacclimation

Photoacclimation is a reversible adjustment of various physiological processes in response to a changing light environment (Sakshaug *et al*., 1987; MacIntyre *et al*., 2002).

Phytoplankton balance their light energy input with their light energy utilization through a number of feedback processes. For example, the cellular concentration of chlorophyll *a,* and other photosynthetic pigments (carotenoids) decreases as the cells acclimate to higher irradiance (MacIntyre *et al*., 2002). During photoacclimation both E_k and $P_{\max}^{\mathrm{Chl}a}$ can adjust (MacIntyre *et al*., 2002), affecting model derived estimates of primary production (Sakshaug *et al*., 1997).

Changes of E_k by a factor of ~3 or more have been observed on time scales as short as hours (Prézelin and Matlick, 1980; Cullen *et al*., 1992a) to as long as seasons (Côté and Platt, 1983; Harrison and Platt, 1986; Kyewalyanga *et al.,* 1998). It is therefore necessary to understand the variability of E_k on similar time and space scales as it influences estimates of primary production. Moreover, the variation of E_k on the time scale of seasons and across biogeochemical provinces (Côté and Platt, 1983; Harrison and Platt, 1986; Kyewalyanga *et al*., 1998) is relevant to major biogeochemical processes (Longhurst *et al*., 1995).

The goal of this thesis is to develop a new method to measure a photoacclimation parameter related to E_k, using the ubiquitous deployments of *in vivo* chlorophyll *a* fluorometers. This method will be applied to data from autonomous oceanographic platforms to provide insight on the temporal and spatial variability of photoacclimation. Before describing the details of the method to measure the novel photoacclimation parameter using *in vivo* fluorometers, a brief overview of *in vivo* fluorescence of chlorophyll *a* will be presented.

1.3 A Background on Fluorescence of Chlorophyll *a*

Measurements and interpretations of *in vivo* fluorescence of chlorophyll *a* have been important in the study of phytoplankton since the method was introduced for oceanographic

applications by Lorenzen (1966). Conventional chlorophyll *a* fluorometers in use today directly measure fluorescence of chlorophyll *a* by emitting blue light in pulses of constant duration and intensity and measuring the red light fluoresced. These excitation and emission colours are chosen because chlorophyll *a* absorbs strongly in the blue, and fluoresces in the red (Falkowski and Raven, 1997). Since all phytoplankton produce chlorophyll *a* pigments, fluorescence of chlorophyll *a* has been conveniently used for over 40 years to describe vertical (Kiefer, 1973; Cullen, 1982; Holm-Hansen *et al*., 2000), and horizontal (Flemer, 1969; Cullen *et al*., 1982; Swertz *et al.,* 1999) distributions of natural phytoplankton populations.

There are other types of active fluorometers that directly probe phytoplankton physiology, such as the Pulse Amplitude Modulated (PAM) fluorometer (Heinz Walz GmbH, Effeltrich, Germany) which measures fluorescence before and during a bright actinic flash of light. This fluorescence technique is well suited for measuring various physiological parameters, but it requires technical expertise to operate and is not typically deployed on environmental monitoring systems.

To the first order, the amount of fluorescence emitted per unit volume and time (F, µmol photons m^{-3} s^{-1}) is expressed by the following equation (Babin et al., 1996a; Babin 2008):

$$F = E_o(PAR) \cdot \overline{a^*_{phy}} \cdot \mathrm{Chl}a \cdot Q^*_a \cdot \phi_F \qquad (2)$$

where E_o(PAR) is the scalar irradiance integrated over the PAR wavebands (µmol photons m^{-2} s^{-1}), $\overline{a^*_{phy}}$ is the spectrally averaged chlorophyll *a* specific absorption coefficient weighted by the PAR wavebands (m^2 (mg Chl*a*)$^{-1}$) (Babin *et al.,* 1996a), Q^*_a is the proportion of fluorescence that is reabsorbed by the phytoplankton (unitless), and ϕ_F is the quantum yield of fluorescence

(photons fluoresced (photons absorbed)$^{-1}$). This relationship holds for sun induced fluorescence (Babin et al., 1996a) as well as fluorescence measured from *in vivo* fluorometers. Note that although the excitation irradiance of *in vivo* fluorometers, such as the WET Labs ECO Pucks^{TM}, is constant, it is not a common practice to quantify their excitation irradiance. Therefore, the symbol F' will be used to distinguish fluorescence measured from *in vivo* fluorometers from *F*. The units of F' will be denoted relative fluorescence units (rfu).

Since conventional *in vivo* fluorometers have a constant light source, E_o(PAR), changes in F' can be attributed to changes in either $\overline{a^*_{phy}}$, Q^*_a, Chl*a*, or ϕ_F. If, however, measurements are taken on relatively short time scales (order of 1 day) in environments where the phytoplankton population does not change significantly, $\overline{a^*_{phy}}$ and Q^*_a are not expected to vary largely (Stramski and Reynolds, 1993; Babin *et al.,* 1996a). Therefore, Eq .(2) can be simplified to:

$$F \propto \text{Chl}a \cdot \phi_F \tag{3}$$

Under these conditions, measurements of $F \cdot \text{Chl}a^{-1}$ would provide relative estimates of the quantum yield of fluorescence (fluorescence yield) (Babin *et al*., 1996a). This enables the use of F' to study changes in fluorescence yield which can provide insights to the physiology of phytoplankton (e.g., Kiefer, 1973; Loftus and Seliger, 1975; Cullen and Renger, 1979; Cullen, 1982; Vincent *et al.*, 1984).

Fluorescence yield predominantly varies strongly and to some extent consistently as a function of irradiance (Kiefer, 1973; Babin *et al.,* 1996a; Morrison, 2003). When a photon is

absorbed by phytoplankton, it will go to photochemistry, fluorescence, or heat dissipation. The associated probabilities of these three fates sum to one (Schreiber *et al.,* 1995; Parkhill *et al.,* 2001). Therefore if the probabilities of photochemistry or heat dissipation increase, the probability of fluorescence decreases, and fluorescence is said to become quenched. Fluorescence quenching due to photochemistry (photochemical quenching: qP) is more pronounced in relatively low light, and decreases with irradiance as photosynthetic reaction centers become saturated (Fig. 2a). Conversely, fluorescence quenching due to heat dissipation (nonphotochemical quenching: NPQ) is more pronounced in relatively high light, and increases as more of the light energy is dissipated (Fig. 2a). NPQ can further be broken down into two components, energy dependent non-photochemical quenching of fluorescence (qE), and quenching of fluorescence associated with inhibition of photosynthesis (qI).

The model developed by Morrison (2003) describes the effect of these three quenching processes on the quantum yield of fluorescence, φ_f. In this model, qP and qE are both exponential functions that exhibit different saturation irradiances; E_k for photochemical quenching, and E_T for nonphotochemical quenching (Fig. 2). Both E_k and E_T act to scale the irradiance at which the maximum φ_f occurs. qI acts to scale φ_f equally across all irradiances (Fig. 2), but its magnitude can vary as a function of irradiance (Morrison and Goodwin, 2010). The Morrison (2003) model, as re-formulated by Schallenberg *et al*., (2008) to include E_k and omit a dimensionless fraction used to represent reaction centers unaffected by NPQ, is given by:

$$\phi_f = \mathrm{qI} \cdot \left[\phi_{fo} + \left(\phi_{f\max} - \phi_{fo} \right) \left(1 - e^{-E_o(PAR)/E_k} \right) \right] \cdot e^{-E_o(PAR)/E_T} \qquad (4)$$

where ϕ_{fo} is the quantum yield of fluorescence in the dark, and $\phi_{f\max}$ is the maximum quantum yield of fluorescence.

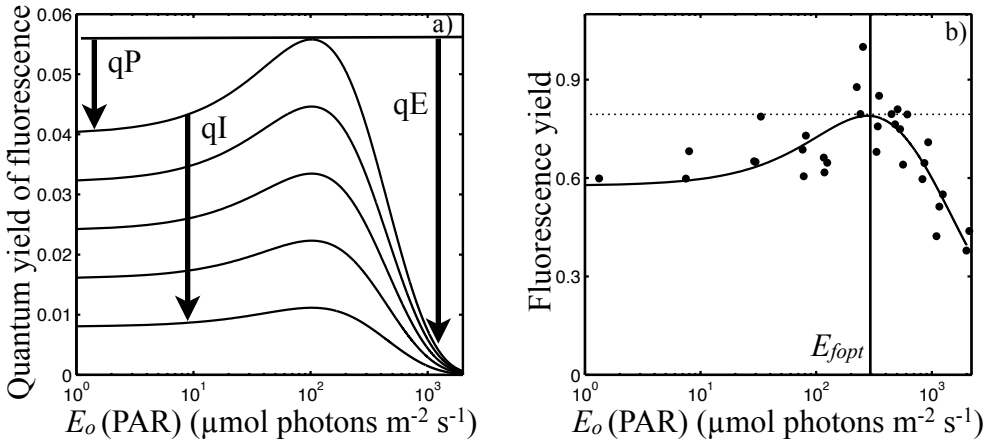

Figure 2. The Morrison (2003) model describes the quantum yield of fluorescence (φ_F) as a function of irradiance. At low irradiance the quantum yield is quenched by photochemistry (qP), which decrease as irradiance increases. At higher irradiance, φ_F is quenched by processes related to heat dissipation (qE). A family of curves is presented in panel a) to demonstrate the effects of qI on φ_F. Panel b). The Morrison (2003) model was scaled and fit to in vivo fluorescence measurements obtained from phytoplankton incubated under various irradiances (Barnett, 2005). The inflection irradiance at the maximum irradiance (E_{fopt}) is provided for reference. In these two panels qI was assumed constant across all irradiances. A dimensionless fraction which leads to a non-zero asymptote at high irradiance, was not included here.

1.3.1 Photochemical quenching of fluorescence

Photochemical quenching of fluorescence denotes the proportion of light energy captured by open reaction centers available for photochemistry (Krause and Weis, 1991). Therefore, in the dark when all reaction centers are open, qP is at a maximum and fluorescence yield is at a minimum. As irradiance increases, the proportion of light energy captured by open reaction centers decreases, qP decreases, and fluorescence yield rises to a maximum (Falkowski and Raven, 1997).

1.3.2 Energy dependent non-photochemical quenching of fluorescence

At high light intensities, the photosynthetic apparatus and other essential cell components can be damaged (Demmig-Adams and Adams III, 1996), therefore phytoplankton have evolved mechanisms to minimize such damage. One such mechanism is the xanthophyll cycle (Demers *et al.,* 1991; Babin *et al*., 1996a; Demmig-Adams and Adams III, 1996; Babin, 2008). When the rate of light absorption is greater than the rate of light energy utilization, a pH gradient across the photosynthetic membrane (i.e., thylakoid) is established (Krause and Weis, 1991; Babin, 2008). Decreased pH in the lumen affects an enzyme that converts diadinoxanthin, a xanthophyll pigment that would normally be used for light harvesting, to diatoxanthin, a xanthophyll pigment that dissipates light energy as heat (Demers *et al*., 1991; Demmig-Adams and Adams III, 1996; Babin, 2008). Diatoxanthin directly competes with chlorophyll *a* for light energy, thereby quenching fluorescence. Since a greater proportion of light energy is being released as heat, this lowers the rate of light energy input to reaction centers and reduces photo-damage (Demers *et al.,* 1991; Babin, 2008), but also fluorescence yield. The direct competition for absorbed light energy from the xanthophyll cycle can lower fluorescence yield by up to 90% (Krause and Weis, 1991). This reduction of fluorescence yield is usually called energy dependent nonphotochemical quenching of fluorescence (qE), and typically occurs on a time scale of seconds and relaxes on time scales of minutes (Demers *et al.,* 1991). When fluorescence yield is plotted *vs.* irradiance, qE can be observed as the sharp reduction of fluorescence yield at high irradiance (Fig. 2; also Morrison, 2003; Barnett, 2005). The reason for the terminology ‘energy dependent’ to describe qE is due to its dependence on the pH gradient across the photosynthetic (i.e., thylakoid) membrane (Krause and Weis, 1991), whereas the terminology ‘non-photochemical quenching’

distinguishes qE and qI from quenching that is dependent on photosynthetic processes (Babin, 2008).

1.3.3 Quenching of fluorescence associated with photoinhibition of photosynthesis

Even though photoprotective processes such as the xanthophyll cycle act to prevent photo-damage, exposure to high irradiance for a relatively long period of time will lead to processes that reduces photosynthesis and also fluorescence, such as downregulation and photo-damage (Horton *et al.*, 1996). One target for photo-damage is the D1 protein in the photosynthetic reaction center. Once damaged, the reaction center must be dismantled and reassembled. Photo-damage to the D1 protein can occur under any irradiance, however it can be repaired, and in low irradiance the damage rate is typically slower than the repair rate, so no net photoinhibition occurs (Adir *et al*., 2003; Ragni *et al*., 2008). Photoinhibition occurs when the rate of damage is faster than the rate of repair (Adir *et al*., 2003).

A damaged reaction center acts as a sink for light energy and further decreases the proportion of light energy going to photochemistry and fluorescence by increasing heat dissipation (Babin, 2008). This process is known as photoinhibitory quenching of fluorescence (qI) and is a form of NPQ. Fluorescence yield can be quenched by up to 40% from qI (Babin, 2008), and its time scale is on the order of 30 min to hours in some natural environments (Vincent *et al.,* 1984). The time scale associated with repairing the damaged reaction center proteins is thought to be on the order of hours (Neale and Richerson, 1987; Oliver *et al.,* 2003) but can change depending on the acclimated state of the phytoplankton (Ragni *et al.*, 2008). Although some models of *F vs. E* treat qI constant across all irradiances (Morrison, 2003; Schallenberg *et al.,* 2008) this assumption is only valid when the rate of mixing across the

irradiance gradient (i.e., mixed layer) exceeds the rate of damage vs. repair (Cullen and Lewis, 1988). This is not likely to be the case with fluorescence yield measured in all natural environments, where inhibitory exposure can vary greatly as a function of ambient irradiance (Vincent *et al*., 1984; Neale and Richerson, 1987; Babin *et al*., 1996a; Oliver *et al*., 2003). Therefore, when analyzing *F vs. E* curves obtained from the natural environment, qI could be more prominent at higher irradiance.

Both qI and qE act to lower fluorescence during high light exposure, but the main process distinguishing the two is time. They are practically defined and hence measured on different time scales; qE on the order of seconds to minutes, and qI on the order of hours (Krause and Weis, 1991, Babin, 2008). Both qE and qI occur in natural environments (Kiefer, 1973; Vincent *et al*., 1984; Neale and Richerson, 1987; Morrison, 2003) and can potentially provide information on harmful light levels for phytoplankton in their natural environment.

1.4 Using Fluorescence Yield to Estimate a Photoacclimation Parameter E_{FT}

Both qP and qE affect the *F vs. E* curve in such a way as to produce an irradiance threshold above which fluorescence yield decreases as irradiance increases (Fig. 2), primarily due to qE. This threshold irradiance has been recognized for a long time (Kiefer, 1973; Kiefer and Reynolds, 1992; Kolber and Falkowski, 1993; Cullen and Lewis, 1995; Cullen *et al.,* 1997; Falkowski and Raven, 1997, Laney *et al*., 2005; Barnett, 2005), and Barnett (2005) obtained a strong correlation between the inflection irradiance of the Morrison (2003) model fit to *in vivo* fluorescence data (E_{fopt}, μmol photons m^{-2} s^{-1}) with the light saturation parameter of photosynthesis, E_k, under a wide variety of simulated environmental conditions. These results are

promising because they provide the framework to use an *in vivo* fluorometer to estimate a parameter directly related to photosynthesis (Barnett, 2005).

Using data from conventional *in vivo* fluorometers, this thesis will present a simple empirical model which estimates the threshold irradiance (E_{FT}, µmol photons m^{-2} s^{-1}) of an *F vs. E* curve (Fig. 3). This model will be referred to as the Empirical Fluorescence Threshold (E.F.T.) model. The first curve describes variations in fluorescence yield under low irradiance. Once a threshold irradiance (E_{FT}) has been reached, fluorescence yield is progressively quenched by qE as irradiance increases (Fig. 3). This model is similar to the model used by Cullen and Lewis (1995), and Holm-Hansen *et al.,* (2000). However, in the present work the E.F.T. model will be fit to *F vs. E* data to explicitly estimate its parameters (see methods section for details), not just to improve Chl*a* estimates, as done by Holm-Hansen *et al.,* (2000).

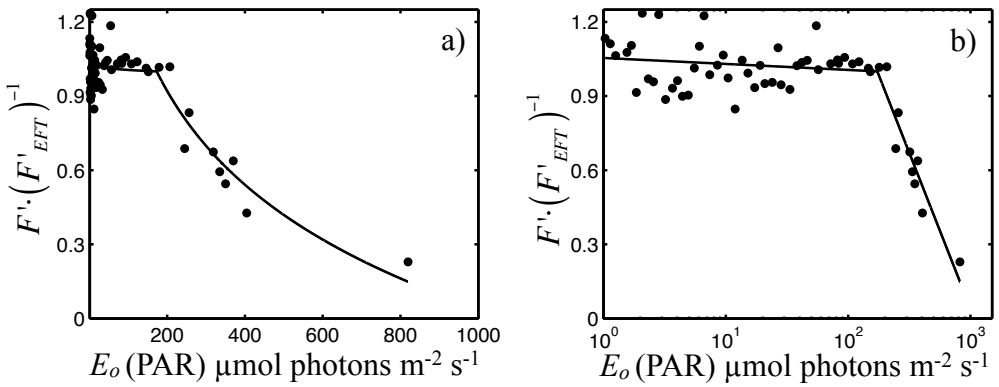

Figure 3. The E.F.T. model consist of two curves joined together at the threshold irradiance E_{FT}. Both panels illustrate the E.F.T. model fit to *F vs. E* data obtained from a vertical profile using an *in vivo* fluorometer, but in panel b) the abscissa is presented in logarithmic space.

Provided that E_{FT} can be reliably related to photosynthetic performance and photoacclimation (see section 3.2) the ability to determine the parameter (E_{FT}) from conventional *in vivo* fluorometers is quite attractive because of the large number of historical datasets which include fluorometers attached to profiling packages (e.g., Conductivity Temperature Depth,

(CTD)), and also more recent data from moorings, ferries, and the increasing number of autonomous moorings optically equipped gliders and profiling floats (Boss *et al*., 2008; Niewiadomska *et al*., 2008; Perry *et al.,* 2008). The time series obtained from these types of observational systems will provide the ability to obtain E_{FT} from natural phytoplankton assemblages on time scales ranging from days to seasons, and examine its empirical relationship with environmental variables.

1.5 Goals of this Thesis

- Demonstrate that robust estimates of E_{FT}, can be obtained from *in vivo* fluorometers, situated on autonomous oceanographic observation systems.
- Describe the variability of E_{FT} on three different time scales, hours, days, and seasons.
- Explain the dominant causes of variability observed in E_{FT}.

Chapter 2: Methods

An empirical model was developed to determine the threshold irradiance (E_{FT}) at which fluorescence yield begins to decrease with increasing irradiance (Fig. 3). This model was applied to an 18 day data set from the SeaHorse™, a moored autonomous vertical profiling CTD (Hamilton *et al*., 1999), and a ~2 year data set from a Land/Ocean Biogeochemical Observatory (LOBO; Satlantic, Inc.) which is a moored autonomous environmental monitoring buoy (Comeau *et al*., 2007; Jannasch *et al*., 2008) to obtain estimates of E_{FT}. In the sections below, the mathematical formulation of the E.F.T. model and the procedures used to apply it to each data set will be described.

2.1 Fluorescence Threshold Parameter and the E.F.T. Model

A least squares non linear curve fitting routine was used to minimize the cost function (sum of squares of the residuals) of the E.F.T. model (Eq. 5) to fluorescence yield and E_o(PAR) data by varying its parameters.

$$F' = \left(\left(F'_{EFT} + m_1 \cdot \ln\left(\frac{E_o(\mathrm{PAR})}{E_{FT}} \right) \right) \cdot \left[E_o(\mathrm{PAR}) < E_{FT} \right] \right) + \left(\left(F'_{EFT} + m_2 \cdot \ln\left(\frac{E_o(\mathrm{PAR})}{E_{FT}} \right) \right) \cdot \left[E_o(\mathrm{PAR}) \geq E_{FT} \right] \right) \quad (5)$$

The E.F.T. model describes two curves that meet at the irradiance E_{FT}. It has four parameters: E_{FT}, fluorescence at the irradiance E_{FT} (F'_{EFT}, rfu), the slope of the first line (m_1, rfu), and the slope of the second line (m_2, rfu). The terms in square bracket are Boolean operators defining the ranges of E_o(PAR). Since this is an empirical model, its parameters are optimized for the range of

irradiance specific to each *F vs. E* curve. If the model were generalized to very high or very low irradiances, eventually it would predict negative values of fluorescence yield.

The least squares curve fitting routine required an initial parameter guess to begin its optimization. Since the optimization can be sensitive to the initial parameters used (Fennel *et al*., 2001), the curve fitting routine was run 100 times on each *F vs. E* curve using randomized initial parameters. The parameters from the iteration which had the minimum sum of squares of the residuals were chosen as the best estimate of the global minimum. Additional details of the E.F.T. model are provided in appendix (A.4)

2.2 Lab Methods

Barnett (2005) determined a positive correlation between E_k, the light saturation parameter for *P vs. E,* and the inflection irradiance of the Morrison (2003) model fit to her data (E_{fopt}) (Fig. 2b). Since E_{fopt} is related to, but not the same as E_{FT}, data from Barnett (2005) were used to demonstrate the relationship between E_{FT} and E_k.

Briefly, the lab experiment from Barnett (2005) was set up as follows: Semi-continuous cultures of *Thalassiosira pseudonana* were grown in modified L1 medium (Guillard and Hargraves, 1993) at 15 ^{o}C under a 14:10 hour light:dark cycle for at least 10 generations prior to experimentation. Acclimated culture conditions included two light (high/low irradiance at 534 μmol photons m^{-2} s^{-1} and 49 μmol photons m^{-2} s^{-1}) and two nutrient treatments (replete/N-limited at 880 μM NO_3^- turbidostat mode and 50 μM NO_3^- chemostat mode) concentrations (cf. Parkhill et al. 2001). Nutrient starvation was explored by allowing acclimated nutrient limited cultures to enter unbalanced growth and starve for 2 or 3 days.

Photosynthesis measurements were obtained from ^{14}C incubations in a Photosynthetron according to a modified method from Lewis and Smith (1983). Twenty-four subsamples from each treatment were exposed to a range of irradiances from 10 µmol photons m^{-2} s^{-1} to 2200 µmol photons m^{-2} s^{-1} for 20 minutes. A semi-empirical model (Platt *et al*., 1980) was fitted to the generated data to retrieve E_k.

A Pulse Amplitude Modulated (PAM) fluorometer combined with a custom-built light box, known as a PAMotron (Parkhill 2003; Barnett, 2005), was used to measure *F vs. E* curves. The light box holds independent subsamples of culture at 12 individual irradiances (~0 µmol photons m^{-2} s^{-1} - 2100 µmol photons m^{-2} s^{-1}) and *in vivo* fluorescence (F'; maximum fluorescence is not reported here) was measured with a weak non-actinic red light source in the presence of background illumination after a 20 minute incubation (Barnett, 2005). It was assumed that, over a 20 minute time period, there were no significant changes in Chl*a*, $\overline{a^*_{phy}}$, or Q^*_a and therefore measurements of F' could be interpreted as relative fluorescence yield as a function of irradiance. Incubation periods were 20 min to match the length of photosynthesis incubations. The E.F.T. model was fit to these *F vs. E* curves to determine $E_{FT\text{-}pam}$. The subscript '*-pam*' indicates that E_{FT} was determined from the PAMotron, to distinguish it from other methods.

2.3 Field Measurements

2.3.1 SeaHorse™

The SeaHorse™ (Hamilton *et al*., 1999) is a moored autonomous profiling CTD also equipped with a LI-COR spherical quantum scalar irradiance sensor (model LI-193SA) to

measure scalar irradiance over the PAR wavelengths as a function of depth ($E_o(z,\mathrm{PAR})$, µmol photons m^{-2} s^{-1}) and a WET Labs WETStar *in vivo* fluorometer. The fluorometer is part of a series of flow-through instruments housed within the system (Hamilton *et al*., 1999). The SeaHorse™ was moored at Station 2 on the Halifax Line (Petrie, 2004), 30 kilometers off the coast of Nova Scotia, Canada, and measured a vertical profile from ~3.5 m to 80 m approximately once every hour. Although the SeaHorse™ was deployed at this location during spring/early summer of 2007, only data from April 2007 (18 days total) will be used in this thesis, since this time period had relatively deep mixed layers that were required to satisfy assumptions, discussed below.

Fluorescence assumption

If Chl*a,* $\overline{a^*_{phy}}$, and Q^*_a, are assumed to be uniform within the surface mixed layer (ℓ, m), then according to Eq. (3), changes in F' within ℓ are proportional to changes in the fluorescence yield. Therefore profiles of F' and E_o(z,PAR) within ℓ can be interpreted as profiles of fluorescence yield vs irradiance of a phytoplankton assemblage (Fig. 4; Eq. 3).

The assumption that Chl*a,* $\overline{a^*_{phy}}$, and Q^*_a are uniform within ℓ is valid when the mixing timescale is short enough to prevent the development of gradients due to differences in the rate of accumulation of biomass, or differences in photoacclimation (Lewis *et al*., 1984; Cullen and Lewis, 1988). For this study, the boundary of ℓ was defined to be the depth at which density exceeds the near surface density by 0.02 kg m^{-3}. Due to sampling limitations of the SeaHorse™ the near surface density was defined as the mean density between 5 m and 7 m depth. E_{FT} was determined from each profile by using F' and $E_o(z,\mathrm{PAR})$ to create an *F vs. E* curve (Fig. 4).

Since the SeaHorse™ profiles the water column once per hour, estimates of E_{FT} can also be obtained hourly, provided there is sufficient irradiance in the water column to induce surface quenching. E_{FT} determined from vertical profiles will be given the symbol $E_{FT\text{-}pro}$ (µmol photons m^{-2} s^{-1}).

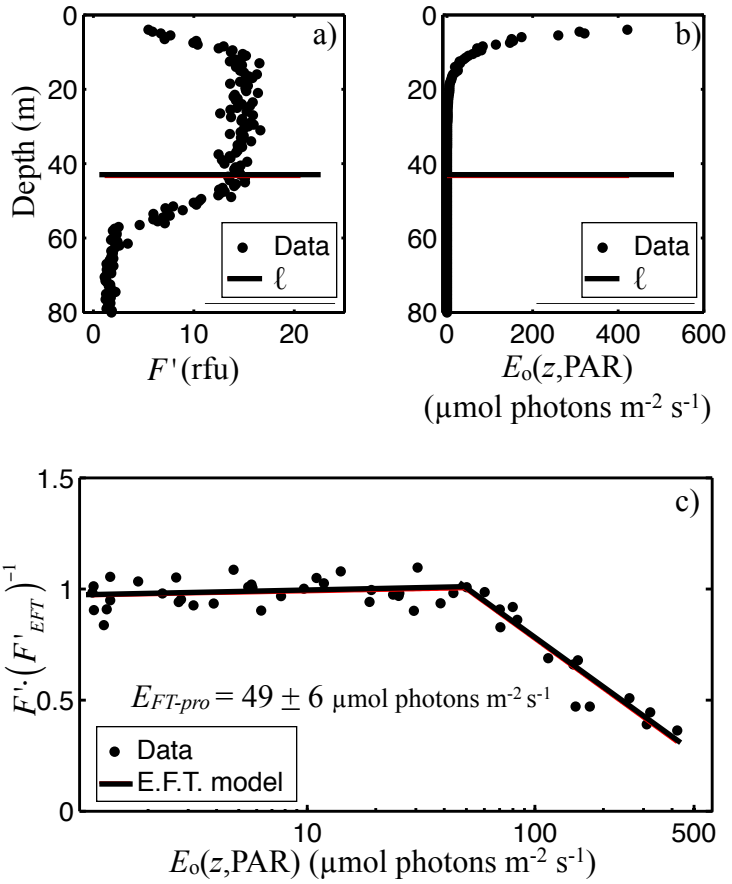

Figure 4. A typical in vivo fluorescence (F') profile, which is assumed to be proportional to fluorescence yield within the mixed layer (panel a) and a typical scalar irradiance profile (panel b) are illustrated along with the depth of the mixed layer (red line). Panel c) The associated *F vs. E* curve obtained with data from F' and E_o(z,PAR). The E.F.T. model was fit to these data and the resulting estimate of E_{FT} ± 1 standard error is displayed.

2.3.2 Land/Ocean Biogeochemical Observatory (LOBO)

The LOBO is a water quality monitoring buoy that measures a suite of environmental variables near the sea surface (~0.3 m) (Comeau *et al*., 2007; Jannasch *et al*., 2008). It has a sampling rate of once per hour, and has been deployed with an irradiance sensor since May 2007

in the Northwest Arm, an urban coastal inlet in Halifax, Nova Scotia, Canada. For this study, near surface F' and total downwelling irradiance above the surface were used to create *F vs*. *E* curves to determine E_{FT} estimated from a surface moored buoy ($E_{FT\text{-}moor}$) (Fig. 5).

Fluorescence yield assumption

It was assumed that day to day changes in F' measured at night (F'_N, rfu), are proportional to changes in the product of $\overline{a^*_{phy}}$, Chl*a*, and Q^*_a according to Eq. (6).

$$F'_N \propto \overline{a^*_{phy}} \cdot \mathrm{Chl}a \cdot Q^*_a \tag{6}$$

Since the time scale for relaxation of qE and qI are on the order of minutes (Demers *et al*., 1991) and hours (Neale and Richerson, 1987; Oliver *et al.,* 2003) respectively, F'_N was measured as the median nighttime fluorescence between the hours of 0100 and 0400 (local) (Fig. 5a;). Changes in F'_N from one night to the next are assumed to represent changes in the variables of Eq. (6), independent of the previous day's irradiance. To examine changes in fluorescence yield, F' can be normalized by F'_N linearly interpolated throughout the day (F'_{Ni}, rfu) (Fig. 5a;). The symbol F'^* (unitless) will be used to designate F' normalized to F'_{Ni} (Fig. 5b). The E.F.T. model was then fit to F'^* and $E_o(0^-,\mathrm{PAR})$ obtained over 7 days to provide one estimate of $E_{FT\text{-}moor}$ (Fig. 5c). This analysis cannot account for short term changes in $\overline{a^*_{phy}}$, Chl*a*, and Q^*_a during the day, which could be caused by advection, nonlinear biological dynamics, or vertical movement of phytoplankton and contribute error to the relationship.

Conversion from $E_d(0^+,\text{total})$ *to* $E_o(0^-,\text{PAR})$

In order to determine physiological parameters of phytoplankton it is important to use scalar irradiance throughout the PAR wavebands, because these are the wavelengths available for photosynthesis. The LOBO buoy, however, measures total downwelling irradiance (285 nm - 2800 nm) above the surface ($E_d(0^+,\text{total})$, W m^{-2}) with an Eppley pyranometer, and it must be converted to photosynthetically available scalar irradiance below the surface ($E_o(0^-,\text{PAR})$, µmol photons m^{-2} s^{-1}). The units were converted from W to mol photons s^{-1} because photosynthesis is a discrete process and the energy for a given photon is of less interest for photosynthesis. Also these are the typical units reported in the modern literature. Downwelling irradiance over the wavelengths 285 nm - 2800 nm was converted to scalar irradiance over the PAR wavelengths by Eq. (7):

$$E_o\left(0^-,PAR\right) = a \cdot \left(1 - r\right) \cdot \tau \cdot E_d\left(0^+,total\right) \tag{7}$$

where $a = 0.45$ is a non-dimensional conversion factor used to limit total spectral irradiance to the PAR wavebands (Kirk, 1994), $r = 0.03$ is a non-dimensional reflection value (Kirk, 1994), and $\tau = 1.15$ is a non-dimensional factor used to convert between downwelling and scalar irradiance (Jerome *et al*., 1988; Schallenberg et al., 2008).

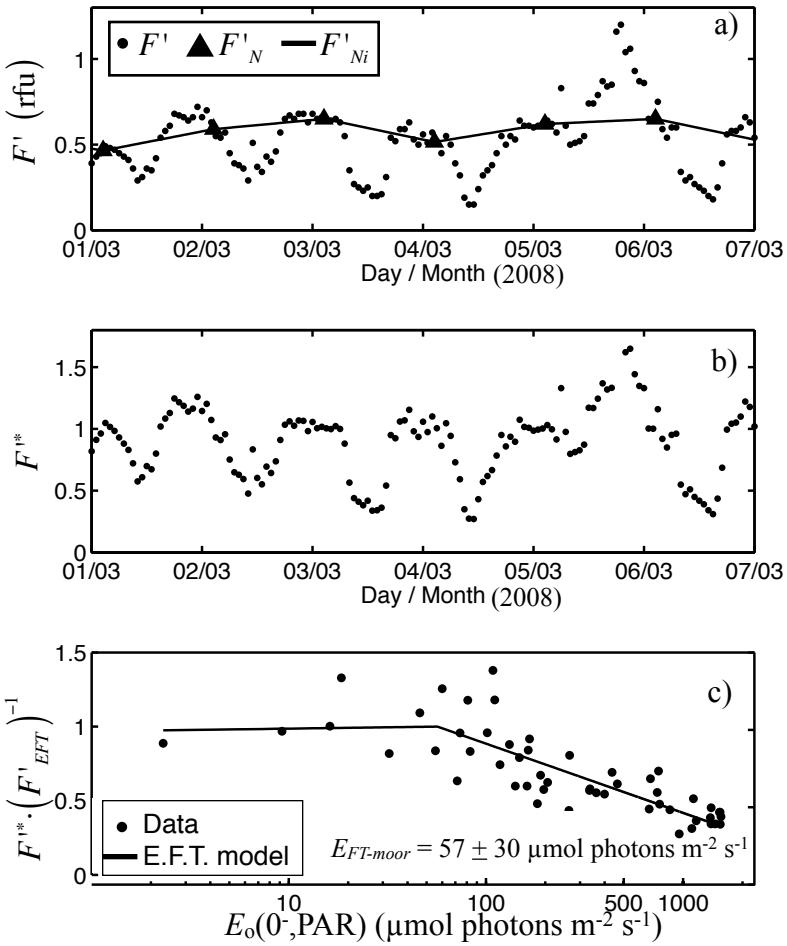

Figure 5. A time series of *in vivo* fluorescence (F') from the LOBO mooring (panel a), with average nighttime data (F'_N) illustrated as triangles, which is assumed to be a measure of F' independent of irradiance. A linear interpolation between each F'_N (F'_{Ni}) provides an estimate of unquenched F' throughout the day. Panel b) An estimate of relative fluorescence yield (F'^*) is obtained by normalizing F' by F'_{Ni}. Panel c) The associated fluorescence yield vs. irradiance with the E.F.T. model fit to it. The resulting estimate of $E_{FT\text{-}moor} \pm 1$ standard error is displayed.

2.4 Quality Control

Estimates of E_{FT} were used only if:

- the curve fitting routine converged and yielded fits with p-values less than or equal to 0.05,

- incident irradiance was sufficiently high to quench $F'\cdot(F'_{EFT})^{-1}$ below 0.65 at the highest irradiance measured, to eliminate cases where there was not enough light to induce sufficient qE,
- the m_1 slope was significantly greater than the m_2 slope (α=0.05). Since this model determines the 'breakpoint' between the two curves, the fit was only trusted if there was a significant difference between these two parameters. In order to statistically compare the slopes m_1 and m_2, the t-statistic was determined by Eq. (8):

$$t = \frac{m_1 - m_2}{\sqrt{\left(S_{m_1}\right)^2 + \left(S_{m_2}\right)^2}} \tag{8}$$

where S_{m1} and S_{m2} are estimates of the standard error for m_1 and m_2. A p-value was determined from this t-value and the degrees of freedom of (n - 4).

These quality controls provide an objective way to eliminate E_{FT} estimates when there is insufficient irradiance, excessive scatter in the *F vs*. *E* curves, or significant error from changes in Chl*a* as a function of irradiance.

Chapter 3: Results

3.1 Uncertainties in Estimating E_{FT}

Each estimate of E_{FT} is obtained from a least squares curve fitting routine that provides uncertainty estimates. For example, when the E.F.T. model is fit to an *F vs. E* curve with considerable scatter, the estimate of E_{FT} will have a greater standard error than a relationship with less scatter (compare the standard errors from Fig. 4c and 5c). In order to examine the uncertainty in the E_{FT} estimates, the relative uncertainties of E_{FT} from each instrument were determined and compared as a percentage (Fig. 6). Out of the three data sets, the SeaHorse™ data provided estimates of $E_{FT\text{-}pro}$ with the lowest relative standard error, a median of 11%. The median percent standard errors were 27% and 32% for the lab PAMotron data set and the LOBO data set respectively.

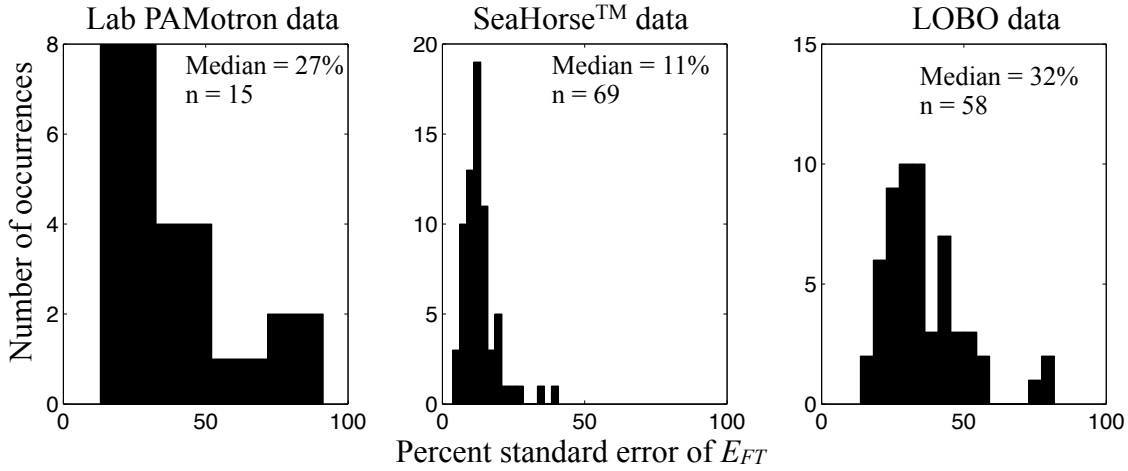

Figure 6. The uncertainty of E_{FT} estimates from each dataset. The dataset that determined E_{FT} with the lowest percent standard error was the SeaHorse™ with a median percent error of 11%. Percent standard error is defined as the standard error normalized by its associated E_{FT} then multiplied by 100.

3.2 Correlation Between E_k and $E_{FT\text{-}pam}$ in Lab Studies

The correlation between $E_{FT\text{-}pam}$, estimated after a 20 min exposure to a range of irradiance, and E_k, estimated from measurements of photosynthesis during similar exposure times was examined (Fig. 7). Since both *P vs. E* curves and *F vs. E* curves were measured from the same phytoplankton culture, both E_k and $E_{FT\text{-}pam}$ are directly comparable. The comparison between $E_{FT\text{-}pam}$ and E_k resulted in a positive correlation with a slope of 2.27 (unitless), and a coefficient of determination of 0.89. Since the slope is not 1:1, these two parameters are not interchangeable. Nonetheless, the correlation over this range of environmental factors provides evidence that $E_{FT\text{-}pam}$ is indeed related to a useful photoacclimation parameter.

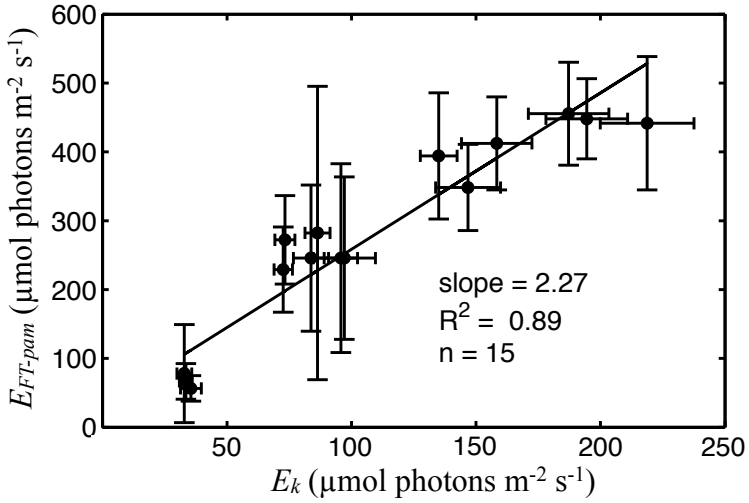

Figure 7. The correlation between $E_{FT\text{-}pam}$ and E_k, from acclimated phytoplankton cultures under a variety of light and nutrient regimes. The error bars represent plus or minus one standard error obtained from their respective curve fitting algorithms, and the line is a Model II geometric mean regression with a coefficient of determination of 0.89 and a slope of 2.27. The estimates of $E_{FT\text{-}pam}$ were determined by applying the E.F.T. model to *F vs. E* curves obtained from Barnett (2005). E_k data were also obtained from Barnett (2005).

3.3 Within Day Variability of $E_{FT\text{-}pro}$

Not all 18 days of the SeaHorse™ deployment were used to examine possible daily patterns of $E_{FT\text{-}pro}$. It is difficult to obtain meaningful $E_{FT\text{-}pro}$ estimates on days with shallow

mixed layers or high cloud cover, and as a result, there were some days which did not produce a quality controlled estimate of $E_{FT\text{-}pro}$. Therefore only days with more than 6 quality controlled $E_{FT\text{-}pro}$ estimates were chosen to examine possible daily patterns (6 days out of 18). The 6 days examined did not provide clear patterns (Fig. 8).

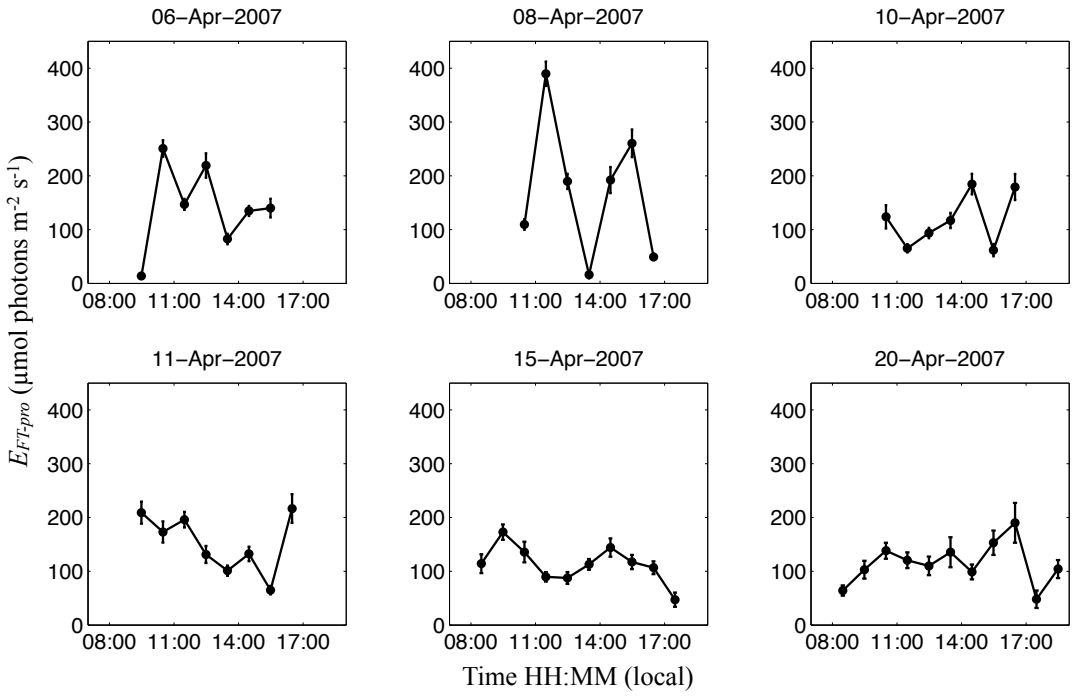

Figure 8. Hourly estimates of $E_{FT\text{-}pro}$ determined from SeaHorse™ profiles for 6 dates in April 2007. In order to properly characterize daily variability, only dates with more than 6 quality controlled $E_{FT\text{-}pro}$ data were used. Error bars on $E_{FT\text{-}pro}$ represent ± 1 standard error, obtained from the curve fitting routine to determine the parameter $E_{FT\text{-}pro}$.

To further examine the daily variability of $E_{FT\text{-}pro}$, the data (Fig. 8), were normalized by their daily mean, and grouped according to when they were sampled (Fig. 9) (morning, 0800 h to 1000 h; mid-morning, 1000 h to 1200 h; noon, 1200 h to 1400 h; afternoon, 1400 h to 1600 h; and evening, 1600 h to 1800 h). An ANOVA performed on these groups provided no evidence to suggest that any of the group means were different from each other (Fig. 9; $p = 0.54$; $n = 50$).

Although the group means do not appear to be different from each other, there was a pattern in the variability of each group (Fig. 9). The midday group had the smallest min-max

range, and interquartile range, while the morning and evening groups have the highest min-max and interquartile range.

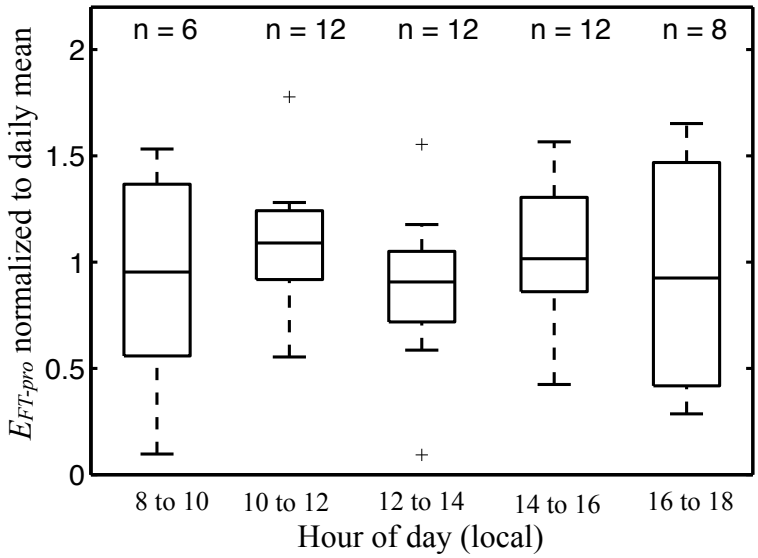

Figure 9. Analysis of the daily variability of $E_{FT\text{-}pro}$. All the values determined from figure (8) were normalized to their respective daily means and grouped according to the time periods shown. The median is the line within the box, the upper and lower limits of the box are the upper and lower quartiles, and the whiskers represent values that are greater than the quartiles but less than 1.5 times the quartiles.

3.4 Seasonal Variations of $E_{FT\text{-}moor}$

The E.F.T. model was used to create a two-year time series of $E_{FT\text{-}moor}$ using 7-day bins of F' and $E_o(0^-,\mathrm{PAR})$ from the LOBO time series (Fig. 5 and 10a). For example, an $E_{FT\text{-}moor}$ estimate was obtained from days 1-7 and the next estimate of $E_{FT\text{-}moor}$ was obtained from days 7-14. The ~2 year LOBO time series provided 58 quality-controlled $E_{FT\text{-}moor}$ estimates from the 102 possible seven-day bins. Seasonal patterns in $E_{FT\text{-}moor}$ are observed (Fig. 10a), where $E_{FT\text{-}moor}$ was lower in the winter and higher in the summer, which followed the seasonal patterns of near surface irradiance (Fig. 10b), nighttime fluorescence (Fig. 10c), and near surface water temperature (data not shown).

The data from figure (10a) were grouped into seasons (Dec-Feb, winter; Mar-May, spring; Jun-Aug, summer; Sept-Nov, fall), to observe the seasonal trends (Fig. 11). An ANOVA comparing the means of each group resulted in a p-value of 0.0046. This provides significant evidence to suggest that at least one seasonal mean is significantly different than the others. A subsequent Tukey-Kramer multiple comparison test determined that the winter mean was significantly different from both the summer and spring means ($p < 0.05$).

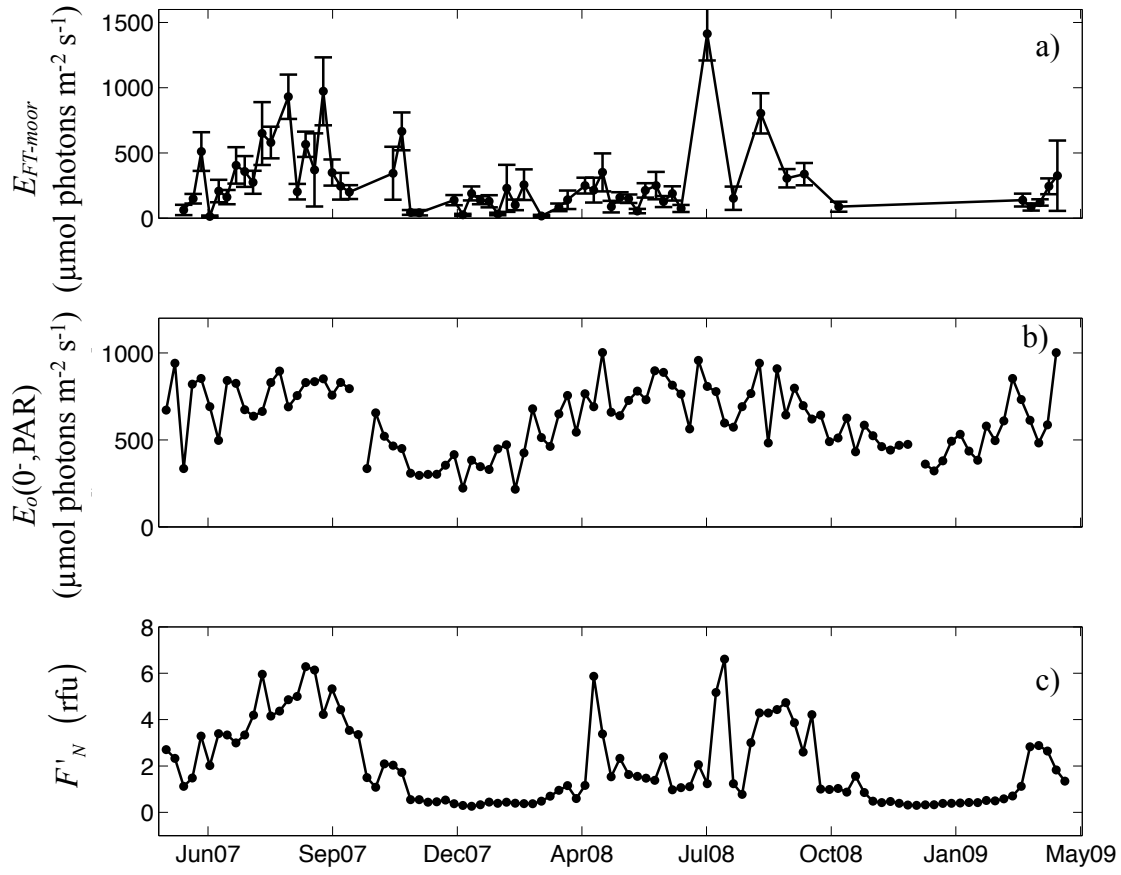

Figure 10. A time series of approximately two years obtained from the LOBO buoy located in the Northwest Arm of Halifax, Nova Scotia, Canada. $E_{FT\text{-}moor}$ was determined from 7-day bins. Only data points that passed the quality control are shown. The error bars represent ± one standard error. Panels b) and c) demonstrate the seasonal variability of near surface irradiance and nighttime fluorescence (F'_N) respectively, where each data point represents a mean over seven days.

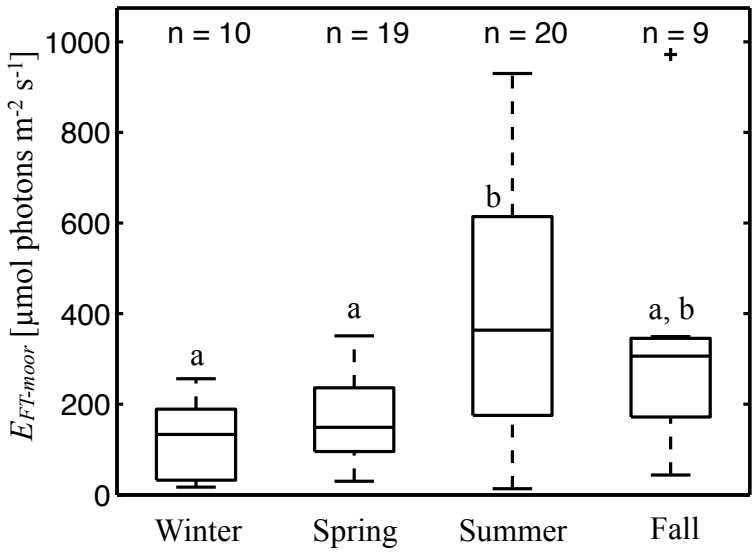

Figure 11. Seasonal variations of $E_{FT\text{-}moor}$. The seasons are grouped as follows: Dec-Feb, winter; Mar-May, spring; Jun-Aug, summer; Sept-Nov, fall. According to an ANOVA and a subsequent Tukey-Kramer multiple comparison analysis, there is evidence (p = 0.0046; n = 58) that the mean winter $E_{FT\text{-}moor}$ is significantly different than the summer and spring seasonal means. Groups with the same letters are not significantly different. See figure (8) for a description of the boxplots.

3.5 Day to Day Variability and Empirical Predictors of $E_{FT\text{-}pro}$

A time series of daily averaged $E_{FT\text{-}pro}$ over an 18 day period in April was created along with the daily averages of relevant environmental variables, such as, $E_o(0^-,\text{PAR})$, the average Chl*a* of the mixed layer ($\overline{Chl_\ell}$, mg Chl*a* m^{-3}), mean mixed layer irradiance ($\overline{E_o(\ell,PAR)}$, µmol photons m^{-2} s^{-1}), and optical depth of the mixed layer (τ_ℓ, unitless) to examine possible trends. See appendix (A.1) and (A.3) for the methods used to determine $E_o(0^-,\text{PAR})$ and $\overline{Chl_\ell}$. The optical depth of the mixed layer was defined as the product of K_o(PAR) and ℓ. The mean mixed layer irradiance was determined by a method presented by Vincent (1983) as shown in Eq. (9):

$$\overline{E_o(\ell,PAR)} = \frac{-\left(E_o(\ell,PAR) - E_o(0^-,PAR)\right)}{K_o(PAR)\cdot\ell} \qquad (9)$$

where $E_o(\ell,\mathrm{PAR})$ is scalar irradiance at the base of the mixed layer (μmol photons m^{-2} s^{-1}).

The SeaHorse™ captured the decline of the spring bloom of April 2007 (Fig. 12b). During this time period $\overline{Chl_\ell}$ decreased from ~15 mg Chl*a* m^{-3} to ~5 mg Chl*a* m^{-3}. However, there were no significant trends in daily averages of the other variables, determined from a linear regression analysis of each time series.

In order to examine possible relationships between daily averaged $E_{FT\text{-}pro}$ and daily averages of the other environmental variables on time scales of variability that could be resolved by the analysis (Fig. 13), the data were detrended with respect to time and analyzed with linear regression. The only variable with a significant regression vs. $E_{FT\text{-}pro}$ was $\overline{E_o(\ell,PAR)}$ with a p-value < 0.01 (Fig. 13). The coefficient of determination (R^2) was 0.42. Although the regression statistics are driven by two high $\overline{E_o(\ell,PAR)}$ data points, these results are encouraging and more data should be collected to determine whether this relationship is robust. It is worth noting that Platt and Sathyendranath (1993) found a significant relationship between E_k and the previous three day irradiance history. It is expected that $E_{FT\text{-}pro}$ would also exhibit such a relationship, however this analysis was not performed due to the small number of resulting independent data points (n = 6).

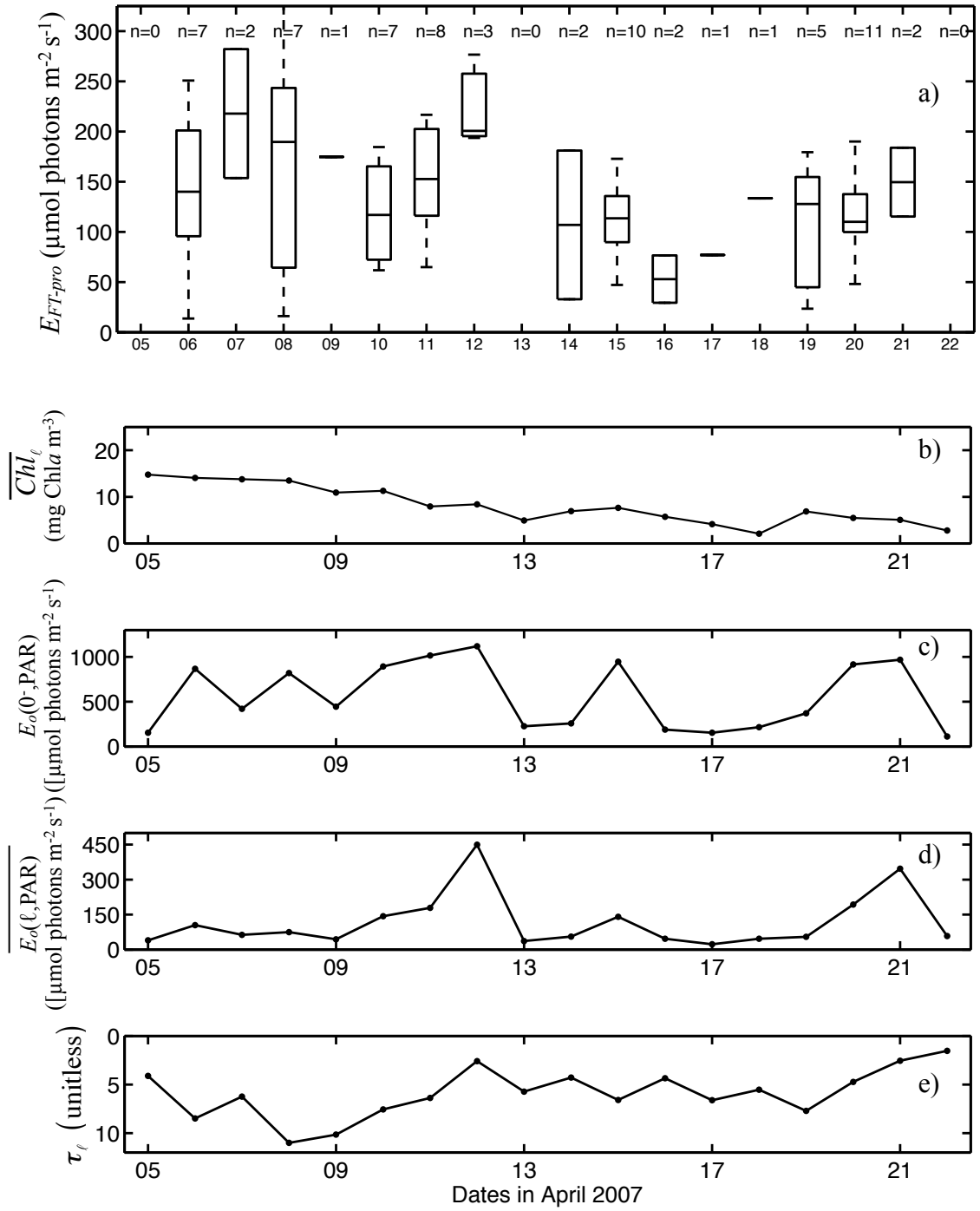

Figure 12. A time series of daily averaged SeaHorse™ data. Panel a) Boxplots of all the quality controlled $E_{FT\text{-}pro}$ estimates were made for each day, see caption of figure (9) for a description of the boxplots. Daily averages of the mean Chl*a* of the mixed layer, near surface irradiance, mean mixed layer irradiance, and optical depth of the mixed layer, for the month of April 2007 are illustrated in panels b), c), d), and e) respectively.

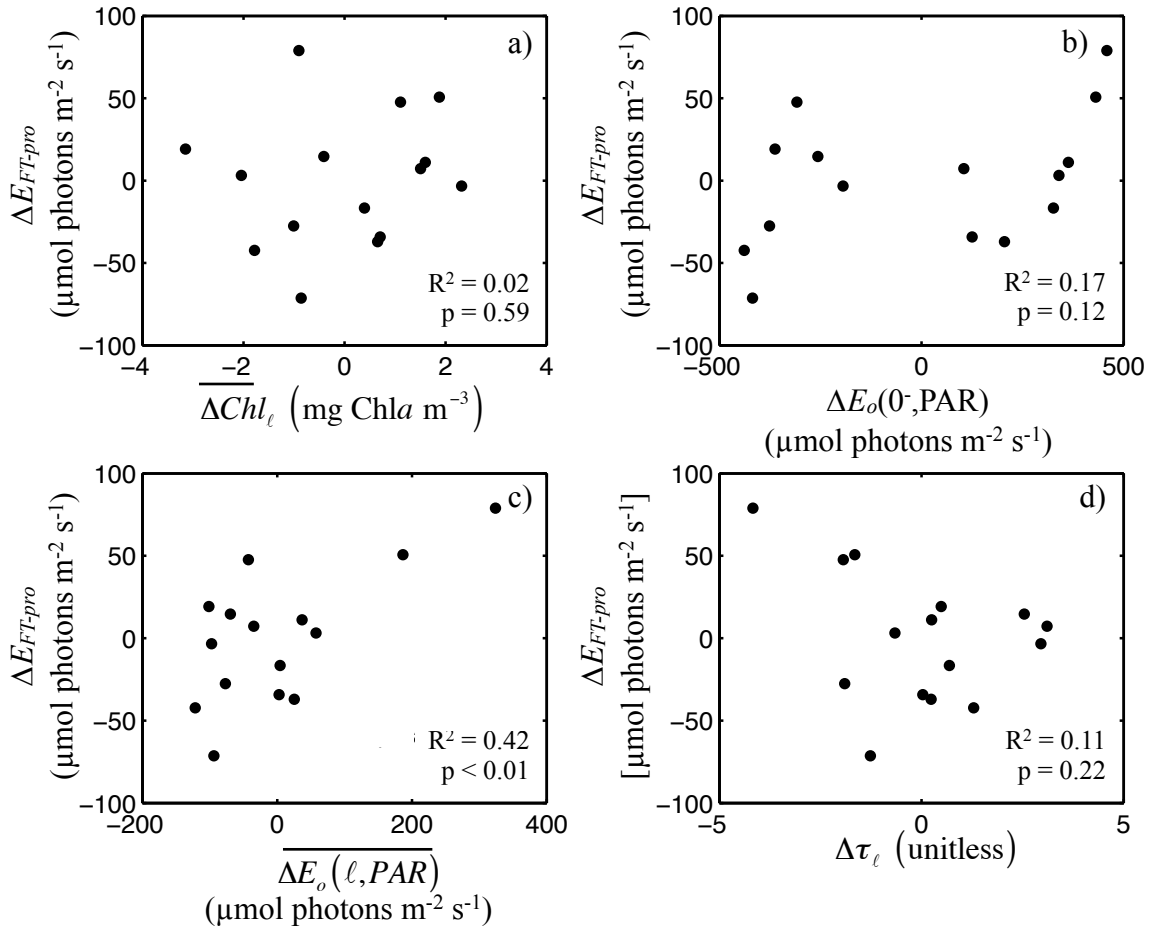

Figure 13. The relationship between the residuals of $E_{FT\text{-}pro}$ and the residuals of mean mixed layer Chl*a*, near surface irradiance, mean mixed layer irradiance, and optical depth of the mixed layer(panels a), b), c), and d) respectively). The residuals were determined by fitting a linear regression model to the time series data (Fig. 12) and subtracting the data from this model. The sample size of each panel is 15. The errors have not been included for clarity.

Chapter 4: Discussion

4.1 Correlation Between E_k and $E_{FT\text{-}pam}$ in Lab Studies

The relationship between E_k and some measure of irradiance at which fluorescence begins to decrease, due to qE, has been previously suggested (Kiefer and Reynolds 1992; Kolber and Falkowski, 1993). Barnett (2005) tested this idea by determining E_k and E_{fopt} from photosynthesis and fluorescence responses of phytoplankton cultures, respectively, to a range of irradiance in parallel incubations. Recall that E_{fopt} is the irradiance at maximum fluorescence of the Morrison (2003) model fit to an *F vs. E* curve (see example in Fig. 2b). These phytoplankton cultures were subjected to a variety of regimes intended to simulate a wide range of environmental conditions: high / low light and nutrient replete/limiting/starved. In this lab study, both E_k and E_{fopt} were positively correlated ($R^2 = 0.78$, n = 18). This supports the initial suggestions that E_k and the irradiance at which fluorescence decreases due to qE are related. Since the Morrison (2003) model could not be fitted to the SeaHorse™ or LOBO data used in this thesis (see discussion below), the E.F.T. model was fit to the lab data provided by Barnett (2005) to retrieve $E_{FT\text{-}pam}$, which was also found to be linearly correlated with E_k (Fig. 7; $R^2 = 0.89$ n = 15, Model II geometric mean regression), with a slope of 2.27 (unitless). Even though the slope of this relationship is not 1 and the underlying relationship may be nonlinear, the correlation between these variables provides the grounds to use $E_{FT\text{-}pam}$ to examine the variability of E_k. Although this relationship looks promising, both E_{FT} and E_k should be measured in the field before this relationship can be generalized to natural environments.

The Morrison (2003) model was originally designed to describe the quantum yield of fluorescence as a function of irradiance. Therefore the shape of the model takes into account the

dominant factors affecting the quantum yield of fluorescence: photochemical and nonphotochemical quenching. In order to apply the Morrison (2003) model to fluorescence measurements obtained from *in vivo* fluorometers, both photochemical quenching and nonphotochemical quenching would have to be apparent in the F' data. Depending on the excitation characteristics of the *in vivo* fluorometer, photochemical quenching may or may not be apparent (compare Fig. 2b with 3b). Photochemical quenching of fluorescence can only be measured if the excitation energy of the fluorometer is sufficiently low so that the photosynthetic reaction centers remain open to provide a minimum fluorescence (Falkowski and Kiefer, 1985; Neale *et al*., 1989). It is not known exactly whether the excitation irradiance of the *in vivo* fluorometers used in this study are sufficiently low to obtain a minimum fluorescence, however it is expected that they overestimate the minimum fluorescence by some unknown extent (Neale *et al.*, 1989). This could be tested by measuring F' from low light acclimated phytoplankton with an *in vivo* fluorometer, and repeated with a neutral density filter placed over the excitation beam of the fluorometer in a similar manner to that described by Parkhill *et al.*, (2001). Since qP is specified in the Morrison (2003) model and it is unknown whether or not qP can be described with the fluorometers used in this thesis, the Morrison (2003) model was not used. Whether or not qP is specified, it should not influence the estimates of E_{FT} since the E.F.T. model predominantly relies on qE (Fig. 3).

Data from the lab study of Barnett (2005) represents only a first step in truly understanding the relationship between $E_{FT\text{-}pam}$ and E_k. Two questions still remain that could be answered with more lab studies. (1) Does this relationship hold with phytoplankton not acclimated to their environment? In natural conditions with varying environmental conditions

associated with perturbations, phytoplankton are unlikely to be fully acclimated to their environment to the same degree that was obtained in the lab study of Barnett (2005) (e.g., Parkhill *et al.,* 2001). (2) Does this correlation between $E_{FT\text{-}pam}$ and E_k remain when different species or mixed assemblages are used? The answers to these two questions will bridge the gap between lab and field studies to further understand how $E_{FT\text{-}pam}$ and E_k relate to each other.

4.2 Assumptions

4.2.1 $E_{FT\text{-}moor}$

To obtain an estimate of fluorescence yield from the LOBO, F'^{*} was obtained by normalizing F' by nighttime fluorescence linearly interpolated throughout the day from one night to the next (F'_{Ni}). This method of estimating fluorescence yield assumed that the combined effects of variability in biomass, species composition, nutritional status and light history change linearly throughout the course of a day. However, many factors lead to changes in F'_{N} from one night to the next (e.g., phytoplankton growth, vertical or horizontal advection, zooplankton grazing, and sinking) which could vary non-linearly throughout the course of a day. Since these processes cannot be accounted for without extensive modeling, it was accepted that the simplified linear interpolation will induce unexplained variability in F'^{*}, and therefore added variability in estimates of $E_{FT\text{-}moor}$ (Fig. 6). Independent measures of Chl*a* throughout the day could be used to check the validity of the linear relationship. The scattering coefficient (m^{-1}), which can be used as a proxy for phytoplankton biomass in certain waters (Loisel and Morel, 1998; and as reported in a discussion forum: Sackmann, *et al*., 2008), was estimated by the LOBO. However, this was not used in the present study because the LOBO is situated in an

estuarine environment, where factors other than phytoplankton strongly affect the scattering signal.

4.2.2 $E_{FT\text{-}pro}$

The assumption that phytoplankton are mixed fast enough in the surface mixed layer to provide a vertically homogenous biomass profile was key to the interpretation that F' is proportional to fluorescence yield (Eq. 3). However, there is a difference between the surface *mixed* layer and the surface *mixing* layer. As Brainerd and Gregg (1995) have described, the surface *mixing* layer is the depth interval that is actively mixing, while the *mixed* layer describes a layer that was mixing at one time to provide a uniform density structure, but may not in fact be currently mixing. With the current instrumentation it was not possible to differentiate between the two, therefore the surface *mixed* layer was obtained through the surface density difference method and assumed to be mixing.

The mixing timescales can be approximated, however. If it is assumed that wind is solely responsible for mixing the surface layer, then an estimate of the mixing time scale for phytoplankton can be obtained by following the method from Denman and Gargett (1983). By using wind data collected from a Sable island meteorological station, and surface mixed layer depths obtained from the SeaHorse™, an estimate of the turbulent friction velocity (w_*, m s^{-1}) was obtained from Eq. (10). It was assumed that this estimate of w_* represents an average value throughout the surface mixed layer and used in Eq. (11) to obtain the mixing time scale of phytoplankton in the mixed layer (t_m, s).

$$w_* = \sqrt{\frac{\rho_a}{\rho_w} \cdot C_{10} \cdot U_{10}^2} \tag{10}$$

$$t_m = \frac{\ell}{2 \cdot w_*} \tag{11}$$

In these equations, ρ_a is a typical air density (1.2 kg m^{-3}), ρ_w is a typical water density (1.025 x 10^3 kg m^{-3}), C_{10} is the drag coefficient of 10 m wind speed on the sea surface (1.3 x 10^{-3} unitless), and U_{10} is the wind speed at 10 m above the water (m s^{-1}).

Using the two equations above will provide only an only order of magnitude estimate of the mixing time scale by assuming only wind forcing and a completely unstratified surface layer. The estimates based on these equations are used in this thesis to determine the range in mixing time scales associated with the average daily winds over the time period measured, to examine whether the mixing time scales compare with the time scale of qI (hours). Using Eq. (10) and (11), a time series of the mixing time scale was created (data not shown), using daily averaged ℓ, and U_{10}. From this time series the minimum and maximum mixing time scales were 6 x 10^2 s (10 min) and 3 x 10^3 s (50 min) respectively (Table 1), which suggest that on windy days qI should be vertically uniform within the mixed layer, but during low winds, some degree of vertical stratification of qI is expected.

Table 1. Mixing time scales (t_m) determined using Eq. (10) and (11) with values for the variables shown. Values for ℓ, U_{10}, and w_*, represent daily means. The dates were chosen because they correspond to the minimum and maximum daily averaged mixing time scales, respectively, during the April deployment of the SeaHorse™.

	11-April-2007	22-April-2007
ℓ (m)	9.5	26.6
U_{10} (m s^{-1})	6.1	3.9
w_* (m s^{-1})	7.6 x 10^{-3}	4.8 x 10^{-3}
t_m (s)	6 x 10^2	3 x 10^3

Examining profiles of nighttime fluorescence from the previous day can provide insight to whether or not the chlorophyll *a* concentration is uniform within the mixed layer. Since the mechanisms responsible for non-photochemical quenching of fluorescence should be relaxed a few hours after the sun sets, fluorescence yield should be uniform within the mixed layer. Therefore, a nighttime F' profile within the mixed layer can be assumed proportional to the Chl*a* profile. To determine whether or not the nighttime F' profile was uniform, nighttime fluorescence profiles were examined (Fig. 14) over the same 6 days corresponding to the subplots in Fig. (8). Of course, one problem that could arise is diel stratification (Neale and Richerson, 1987; Cullen *et al*., 1992a). Even if the water column was mixed during the nighttime, the sun can provide enough heat to stabilize the upper water column during the day. In this case, a nighttime fluorescence profile would provide little information on vertical chlorophyll *a* structure during the following day. The potential for diel temperature stratification was examined (Fig. 15). Diel temperature stratification was evident, particularly April 8th, 10th, and 11th, and slightly on 15th and 20th. This provides evidence that the water column was not actively mixing during the day which suggests the possibility of the development of vertical

gradients of Chl*a*, or at least qI. This is, in part, why the quality control (see section 2.4) was applied to the E.F.T. model to ensure confidence in estimates of E_{FT}. After the quality control checks, the resulting *F vs. E* curves exhibited a pattern consistent with that expected when qE is the dominant factor affecting F' in high light. If obvious vertical structure of Chl*a* were present, the resulting *F vs. E* curve would not pass the quality control check.

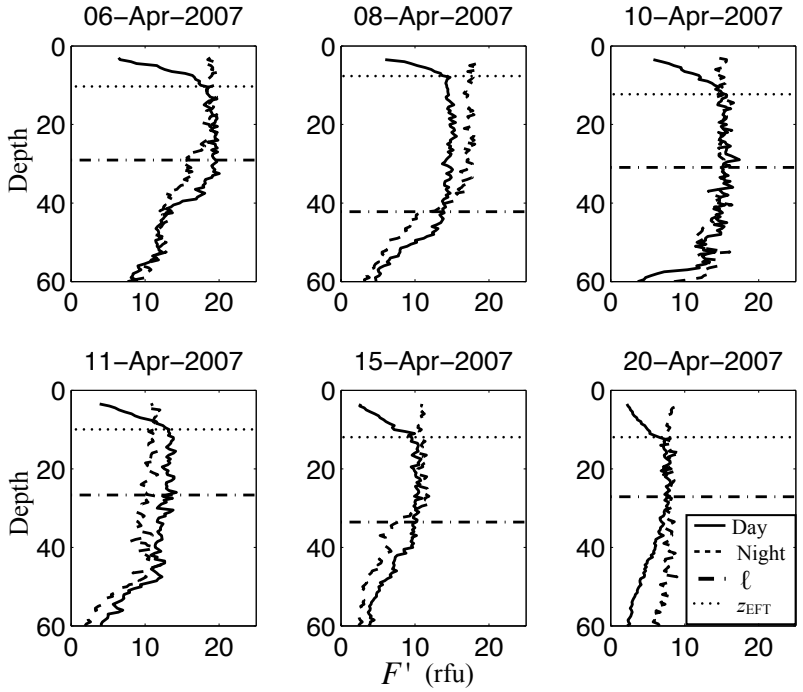

Figure 14. Average profiles of daytime (0900 h to 1500 h, local, solid line) and nighttime (0100 h to 0400 h, local, dashed line) fluorescence from the SeaHorse™. The mixed layer depth is an average of night and daily values (dotted and dashed line). The approximate location of the depth at which $E_{FT\text{-}pro}$ occurs (z_{EFT}) is illustrated by the dotted black line. The dates correspond to each subplot of figure (8).

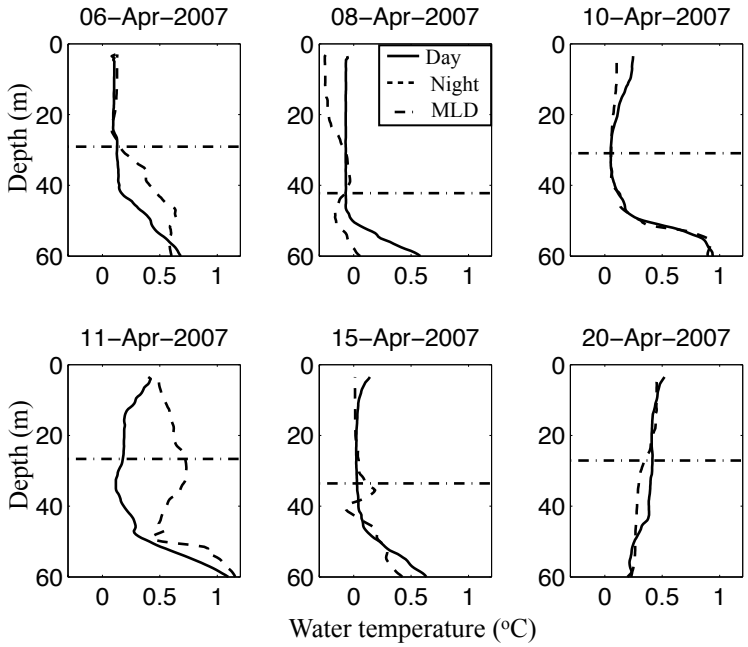

Figure 15. Average daytime and nighttime water temperature profiles obtained from the SeaHorse™. Daytime and nighttime means were determined in a similar fashion as figure (14).

4.2.3 qI independent of irradiance

Previous work studying variability in fluorescence yield has assumed qI to be constant across all irradiances for the data sets analyzed (Morrison, 2003; Barnett, 2005; Schallenberg *et al*., 2008; but see Morrison and Goodwin, 2010 for another method). This is a valid assumption in lab experiments where a phytoplankton culture is subsampled from a population of similar light history (Barnett, 2005). However, in natural environments the effect of qI is difficult to assess (but see Vincent *et al.,* 1984; and Oliver *et al.,* 2003 for fluorescence-based methods). In the water column, there could be a vertical gradient of qI even when some degree of vertical mixing is present (Vincent *et al.,* 1984; Oliver *et al*., 2003). Therefore, even when choosing to use fluorescence measurements within the mixed layer with the SeaHorse™ data, there is still the possibility that qI has influenced F' near the sea surface. In addition to a vertical gradient of qI, there could also be a temporal pattern in the surface waters, i.e., a low effect in the morning, a

high effect in the afternoon, and a decreased effect in the evening (Vincent *et al.,* 1984; Oliver *et al*., 2003).

But what happens to the estimates of E_{FT} if the assumption of constant qI across all irradiances is violated? In the examples provided above, qI is likely to have a smaller influence on low light F' and a greater influence on high light F' (Fig. 16). This quenches high irradiance F' and therefore leads to an underestimate E_{FT} (Fig. 16 and appendix (A.2)). Although the extent to which E_{FT} is lowered is not known and likely variable, the Morrison (2003) model can be used to simulate the effects of various functions of qI *vs.* irradiance see appendix (A.2). An example is provided (Fig. 16), where qI decreases linearly as a function of irradiance (qI=1 at 0 µmol photons m^{-2} s^{-2} and down to qI=0 at 2000 µmol photons m^{-2} s^{-1}). In this example, E_{FT} is lowered by 67 µmol photons m^{-2} s^{-1} or 26% of the estimate of E_{FT} not influenced by qI. Note that the subscripts "-pro" and "-moor" were not used in the above discussion since the effects of qI apply to both.

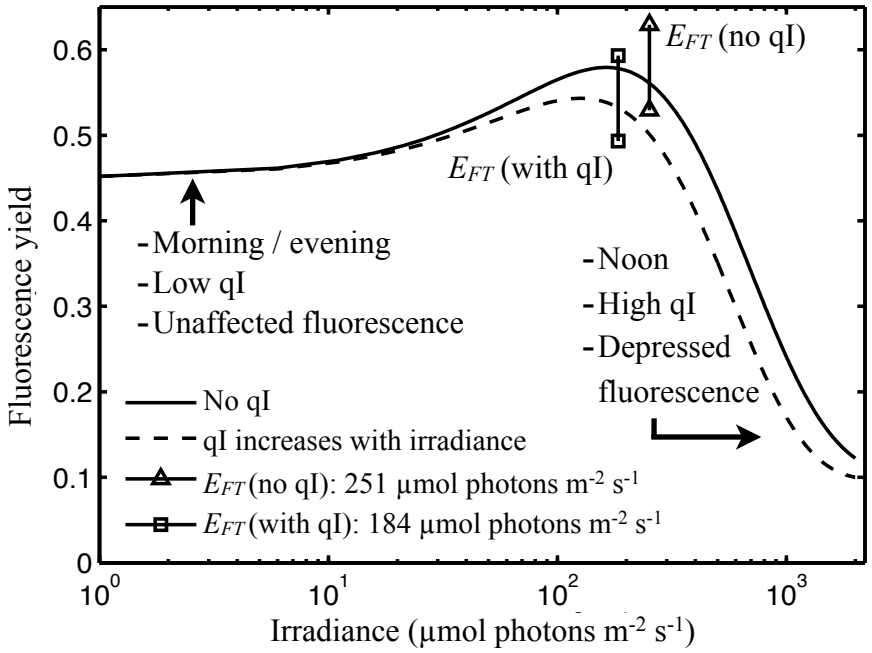

Figure 16. Using the Morrison (2003) model to simulate the effects of qI on an *F vs. E* curve. The low light values represent surface fluorescence data obtained in the morning and high light values represent surface fluorescence data obtained around solar noon. Note that the low light and high light data would have different light histories. qI is constant across all irradiances in the solid line, and qI varies as a function irradiance in the dashed line (see text for details). The E.F.T. model was fit to both curves to estimate of E_{FT}. The estimate of E_{FT} was smaller for the curve with qI varying as a function of irradiance.

4.3 Differences Between $E_{FT\text{-}pro}$ and $E_{FT\text{-}moor}$

The time scales associated with obtaining sufficient data to determine E_{FT} from a profile ($E_{FT\text{-}pro}$) and a surface mooring ($E_{FT\text{-}moor}$) are different. A SeaHorse™ profile is recorded on the order of minutes, while $E_{FT\text{-}moor}$ is determined on the order of days, due to the limited sampling frequency (1 h^{-1}) and the daily cycle of the sun. Do both methods of estimating E_{FT} provide the same result?

Since the SeaHorse™ profiles the water column once per hour, F' and E_o(z,PAR) data chosen from the same depth each hour over a given time period can be used to generate an *F vs. E* curve to obtain $E_{FT\text{-}moor}$. Since $E_{FT\text{-}pro}$ and $E_{FT\text{-}moor}$ are determined from the same instrument,

they can be directly compared (Fig. 17). For the comparison, only $E_{FT\text{-}pro}$ estimates between 1100 h and 1300 h (Fig. 17a; stars) were chosen to determine 4 day averages, since noontime estimates of $E_{FT\text{-}pro}$ are representative of the daily mean (Fig. 9). Since there were only 4 independent data points available to compare $E_{FT\text{-}pro}$ and $E_{FT\text{-}moor}$ (Fig. 17b), a robust comparison was not possible, however, the data did not stray far from a 1:1 line. Although more data are needed, this preliminary comparison suggests that both $E_{FT\text{-}pro}$ and $E_{FT\text{-}moor}$ are directly comparable.

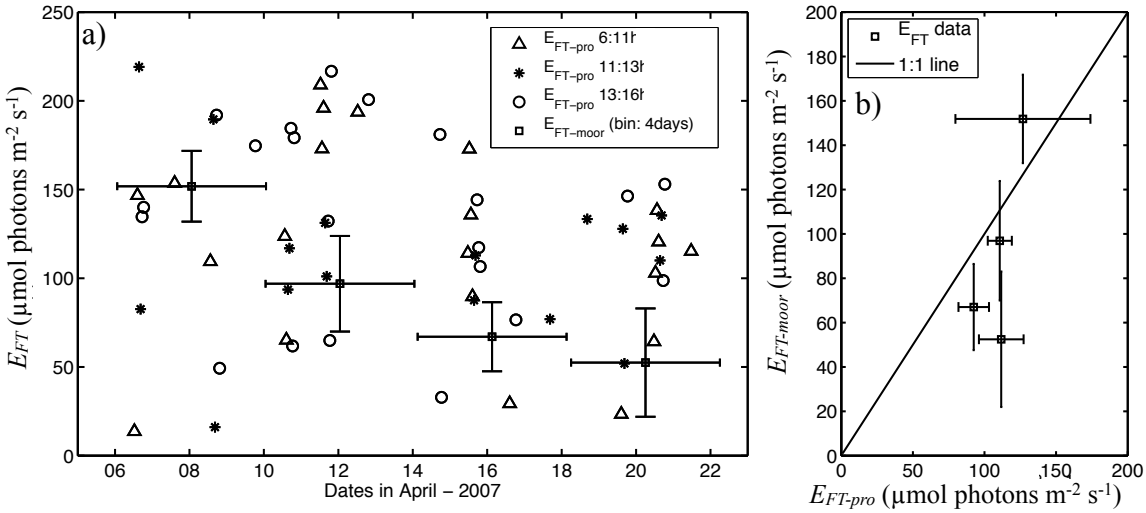

Figure 17. A comparison between E_{FT} determined using the profile method ($E_{FT\text{-}pro}$) and E_{FT} determined from the mooring method ($E_{FT\text{-}moor}$) using SeaHorse™ data. Panel a) Estimates of $E_{FT\text{-}pro}$ were grouped according to shape (triangles for morning estimates, stars for noon time estimates, circles for afternoon estimates, all times local). Estimates of $E_{FT\text{-}moor}$ are also plotted for this time period (squares). A bin size of 4 days was used to determine $E_{FT\text{-}moor}$, at a depth of 4 m. The vertical error bars represent ± 1 standard error and the horizontal error bars represent the time interval over which $E_{FT\text{-}moor}$ was determined. Panel b) Comparison of 4 day averages of noon time $E_{FT\text{-}pro}$ to the 4 day bins of $E_{FT\text{-}moor}$. Vertical error bars represent the standard error of the 4 day means, and the horizontal error bars represent the standard error of each $E_{FT\text{-}moor}$ estimate. A 1:1 line is provided for reference.

4.4 Within Day Variability of $E_{FT\text{-}pro}$

No significant daily patterns of $E_{FT\text{-}pro}$ were observed in this study (Fig. 9). This is consistent with other studies that measured E_k over the course of a day (Harding *et al.,* 1982; Harrison and Platt *et al.*, 1986). However, daily patterns of E_k have been observed in stratified

waters (Cullen *et al.,* 1992a), where E_k is low in the morning and evening and high in the afternoon. The method presented here cannot determine $E_{FT\text{-}pro}$ in stratified waters with the instrumentation available. However, this could be possible if independent simultaneous measures of Chl*a* were available.

In order to estimate $E_{FT\text{-}pro}$ using the SeaHorse™, it was assumed that qI was uniform with depth. If this assumption failed and a vertical structure of qI developed, it would lead to underestimates of $E_{FT\text{-}pro}$ (Fig. 16). The afternoon hours are the most likely time for the assumption of vertically uniform qI to be violated. Therefore, even if the *true* noon $E_{FT\text{-}pro}$ estimates are higher than the other time periods, the underestimate provided by the *estimated* $E_{FT\text{-}pro}$ could hide the pattern.

A temporal pattern was observed in the variance of $E_{FT\text{-}pro}$ when it was normalized and binned into time slots (Fig. 9). The min-max and interquartile ranges were greater in the morning and evening groups than in the midday group. A possible explanation could be linked to the low solar irradiance in the morning and evening. Although the $E_{FT\text{-}pro}$ data presented have been quality controlled, obtaining $E_{FT\text{-}pro}$ from a profile with a small range of irradiance will lead to greater uncertainty in $E_{FT\text{-}pro}$ due to the curve fitting process. The reduced variability around noon leads to a practical application. If a representative daily mean of $E_{FT\text{-}pro}$ is desired, the best time to sample would be around noon.

4.5 Seasonal Variations of $E_{FT\text{-}moor}$

There are many oceanographic monitoring buoys located throughout the world, and their main purpose is not to determine estimates of photoacclimation parameters. This thesis provides an example of how such buoys can develop a time series of $E_{FT\text{-}moor}$ (Fig. 10), a parameter that

relates to E_k (Fig. 7). Studying the $E_{FT\text{-}moor}$ time series provided by these buoys will help us better understand the factors responsible for its variability, and therefore help us to better parameterize E_k in models of primary productivity.

Statistically significant seasonal patterns of $E_{FT\text{-}moor}$ were observed (Fig. 11; $p = 0.0046$; $n = 58$) in the LOBO time series. They followed the expected pattern of photoacclimation over seasons, low in the winter and higher in the summer (Côté and Platt, 1983; Krupatkina *et al.,* 1991).

There are fewer estimates of $E_{FT\text{-}moor}$ (Fig. 10a) in the winter because the ambient mean irradiance is generally low (Fig. 10b) and does not provide sufficient irradiance to induce qE mechanisms which lower fluorescence. Without sufficient high light to quench fluorescence, it is not possible to obtain estimates of $E_{FT\text{-}moor}$. This is an inherent limitation of the E.F.T. model since it relies on *in situ* conditions. The traditional *P vs. E* incubation technique does not have this limitation, since it utilizes artificial light. If desired however, water samples could be obtained and analyzed with the PAMotron or similar device (Johnson, 2004) to obtain estimates of $E_{FT\text{-}pam}$ during the winter.

4.6 Empirical Predictors of Daily Averaged $E_{FT\text{-}pro}$

Other studies (Côté and Platt, 1983; Goebel and Kremer, 2007) have had difficulties in determining the dominant environmental variables responsible for variations in the photosynthesis parameter E_k. Nonetheless the correlation between E_{FT} and $\overline{E_o(\ell, PAR)}$ was significant ($p < 0.001$; $n = 15$) and the coefficient of determination was moderate ($R^2 = 0.42$) (Fig. 12). This correlation seems to be driven by two data points. There is no objective reason to

remove these data, however if removed, the correlation becomes insignificant ($p > 0.1$; $n = 13$). In order to properly assess this correlation, more high $\overline{E_o(\ell, PAR)}$ values are needed.

4.7 Applications for E_{FT}

Although the emphasis of this thesis has been placed on using E_{FT} to understand variations in photoacclimation to ultimately improve primary production estimates, there are other useful applications. One such application is utilizing E_{FT} to obtain better estimates of chlorophyll *a* concentrations from fluorometers. Both Cullen and Lewis (1995) and Holm-Hansen *et al*., (2000) provided a method which uses a similar E.F.T. model applied to their entire data set, to obtain an average E_{FT} and improve estimates of chlorophyll *a* concentration from *in vivo* fluorometers. The method presented here can determine quality controlled estimates of $E_{FT\text{-}pro}$ from individual profiles, and therefore, there is no need to take an average $E_{FT\text{-}pro}$ over many days. Data from the SeaHorse™ demonstrates that the daily mean $E_{FT\text{-}pro}$ can decrease by a factor of ~2-3 in a week (Fig. 12), which implies that significant variability of $E_{FT\text{-}pro}$ can occur on short time scales. By using this method to determine the variability of E_{FT}, the Holm-Hansen *et al*., (2000) method of estimating chlorophyll *a* concentration from *in vivo* fluorescence could be improved (Cullen and Lewis, 1995).

Since measurements of fluorescence can provide unique physiological information about phytoplankton in their natural environment, the reasons for its variability should be quantified and understood. In recent years, increased research efforts have been oriented toward using sun-induced fluorescence measurements for the assessment of nutrient limitation (Letelier *et al.*, 1997; Schallenberg *et al.*, 2008, Behrenfeld, *et al.*, 2009). However, it is necessary to understand, that in order to assess nutrient limitation from measurements of fluorescence, its other sources of

variability must first be accounted for. Fluorescence of chlorophyll *a* from phytoplankton is similar to blood pressure of humans; knowing its variability provides a useful diagnostic but does not necessarily specify the underlying causative factor(s) (*pers. comm.,* Ibarra, 2009). Before one can assess nutrient limitation from fluorescence, characterization of all other factors contributing to its variability must be assessed. This is where E_{FT} measurements are useful. They provide a useful parameter that can be applied to models of fluorescence to explain some of the variability in fluorescence, bringing us closer to understanding of the underlying causes of its overall variability.

4.8 Future work

This thesis research has answered some questions but also created others. Following is a list of three ideas that should be pursued in the near future:

- Gliders and floats. The simple requirements of this model make it applicable to the new generation of optically equipped gliders and profiling floats (Boss *et al*., 2008; Niewiadomska *et al*., 2008; Perry *et al.,* 2008). Being able to direct these observational systems to different water masses and obtain meaningful physiological measurements of phytoplankton will bring unprecedented understanding of how phytoplankton acclimate to their environment (as mentioned in a discussion forum: Sackmann *et al*., 2008).
- qI. Future emphasis should be placed on parameterizing qI so that its variability can be described within the day for fixed depth measurements, and within the water column in stratified environments, as in Oliver *et al.,* (2003) and Ragni *et al*., (2008).
- Extending lab studies to natural environments. A strong correlation between $E_{FT\text{-}pam}$ and E_k was demonstrated in this thesis, providing evidence that there is a relationship between the

two variables. If such relationships are to be generally applied to natural mixed assemblages of phytoplankton, they must be rigorously tested with data from the natural environment.

4.9 Conclusions

It has been known for many decades that *in vivo* fluorescence yield from phytoplankton varies as a function of irradiance. At low irradiance fluorescence yield generally increases until a certain threshold irradiance, when it decreases as irradiance increases. An empirical model was developed to describe this behaviour and extract the irradiance threshold parameter (E_{FT}). It has been hypothesized that this parameter is related to the light saturation parameter of photosynthesis (E_k) (Falkowski and Raven, 1997), and their strong correlation has been presented in this thesis.

A key strength of the parameter E_{FT} is its ability to be readily determined in the natural environment with simple, low cost, ubiquitous instrumentation (an *in vivo* fluorometer and an irradiance sensor). Two methods were described to obtain this parameter: one from a vertical profile ($E_{FT\text{-}pro}$), the other from a fixed depth fluorescence time series, typically obtained from autonomous environmental moorings ($E_{FT\text{-}moor}$). There are advantages and disadvantages associated with each method, and they mainly relate to the time scale of the measurement (vertical profile method, order of minutes; fixed depth method, order of days).

Different time scales of variability in E_{FT} were examined, and the following conclusions were drawn:

- Noon appears to be the best time of day to sample to obtain a precise estimate of daily averaged $E_{FT\text{-}pro}$.

- Although environmental parameters such as daily-averaged Chl*a*, optical depth, and surface irradiance, explained very little of the variability of $E_{FT\text{-}pro}$, a significant correlation was obtained between daily averaged $E_{FT\text{-}pro}$ and mean mixed layer irradiance. However, more data should be collected to determine the robustness of this relationship.
- $E_{FT\text{-}moor}$ exhibited seasonal variability where the winter and spring seasonal means were lower than the summer and fall means.

In addition to qE, qI also affects measurements of fluorescence yield obtained in the natural environment. Since it is difficult to distinguish between the two without more sophisticated methods, qI was assumed constant over the entire *F vs. E* curve. It was shown that when this assumption fails and qI varies according to some function of irradiance, E_{FT} can be underestimated. qI not only affects fluorescence yield estimates obtained from *in vivo* fluorometers, but also sun induced fluorescence. Therefore, care must also be taken when interpreting *F vs. E* curves of sun induced fluorescence.

The "profiling" and "moored" approaches used in this thesis to determine E_{FT} are useful not only for the data sets analyzed herein, but also for many oceanographic missions where time series of fluorescence are obtained, from vertical profiles, glider or ferry transects, or stationary measurements. The methodologies developed in this thesis have the potential to form a powerful new tool that permits more meaningful interpretation of fluorescence profiles and enhances our ability to establish relationships between photoacclimation and environmental variables in different biogeochemical provinces on many temporal and spatial scales.

Appendix

A.1 Propagating SeaHorse™ Irradiance Profiles to the Sea Surface

Surface irradiance $E_o(0^-,\mathrm{PAR})$ and the mean irradiance of the mixed layer $\overline{E_o(\ell,PAR)}$ are two variables used in this thesis, however the SeaHorse™ rarely sampled above 3.5 m during its deployment in April, 2007. $E_o(0^-,\mathrm{PAR})$ was determined by fitting a linear regression model (Eq. a1) to a profile of the natural log of $E_o(z,\mathrm{PAR})$ from the shallowest depth (~3.5 m) to the depth of the 1% light level, to determine its two parameters, $E_o(0^-,\mathrm{PAR})$, and $K_o(\mathrm{PAR})$.

$$\ln\left(E_o(z,PAR)\right) = \ln\left(E_o\left(0^-,PAR\right)\right) - K_o(PAR)\cdot z \qquad \text{(a1)}$$

The parameters $E_o(0^-,\mathrm{PAR})$, and $K_o(\mathrm{PAR})$ were then used to propagate the irradiance profile from the shallowest depth sampled to the surface.

There are problems when using $E_o(z,\mathrm{PAR})$ to determine $K_o(\mathrm{PAR})$ because different wavelengths throughout the PAR wavebands have different attenuation coefficients (Kirk, 1994). For example, near the surface, the high attenuation coefficient of red light will contribute to $K_o(\mathrm{PAR})$, but since there is practically no red light at deeper depths, its attenuation will not contribute to $K_o(\mathrm{PAR})$ near the bottom of profiles. In contrast, blue and green light have lower attenuation coefficients relative to the other colors, therefore they contribute to $K_o(\mathrm{PAR})$ throughout most of the well-lit water column. This leads to higher values of $K_o(\mathrm{PAR})$ near the surface than at depth, even in optically uniform waters. Since the measurements of $E_o(z,\mathrm{PAR})$ only begin from ~4 m, $K_o(\mathrm{PAR})$ is underestimated, resulting in underestimates of $E_o(0^-,\mathrm{PAR})$. In the context of this thesis, the resulting effects were deemed minor.

A.2 Effects of qI on Determining E_{FT}

When photoinhibition (qI) is variable over the *F vs. E* curve, it can lead to underestimates of E_{FT} (Fig. a1). qI is likely to be pronounced around noon, and near the surface in stratified or relatively slowly mixing environments (Oliver *et al.,* 2003). If this is the case, then E_{FT} estimates obtained from the SeaHorse™ on cloudless days around noon and estimates obtained from the LOBO are likely underestimated to some extent due to qI. Although a model of fluorescence quenching related to inhibition of photosynthesis *vs. E* has been published (Neale and Richerson, 1987), since qI is a function of both light exposure (μmol photons m^{-2}) and recovery times (s^{-1}) (Oliver *et al.,* 2003), it is difficult to obtain the exact qI *vs. E* function for phytoplankton in dynamic environments. In order to estimate the extent to which qI can influence E_{FT}, a range of qI *vs. E* functions were examined (Fig. a1).

The influence of qI on E_{FT} was examined using the Morrison (2003) model to create an *F vs. E* curve with different values of qI at each irradiance, then running the E.F.T. model on the resulting *F vs. E* curve. For this analysis, 4 functions of qI *vs. E* were used: qI constant across all irradiances, qI decreases linearly to 0 after the threshold irradiance for nonphotochemical quenching, E_T (Neale and Richerson, 1987), qI decreases logarithmically, and qI decreases exponentially after E_T (Neale and Richerson, 1987). Each estimate of E_{FT} where qI behaved as a function of irradiance was slightly lower than the control case where qI was left constant. The qI *vs. E* function used by Neale and Richerson (1987) provided the greatest E_{FT} underestimate ([252 μmol photons m^{-2} s^{-1} - 240 μmol photons m^{-2} s^{-1}] / 252 μmol photons m^{-2} s^{-1}; ~5%) of the three functions shown. The qI *vs. E* functions presented are to be interpreted as a proof of concept that a qI *vs. E* function can influence estimates of qI. Careful work is required to

properly describe qI in the particular environment studied (Oliver *et al*., 2003; Ragni *et al*., 2008).

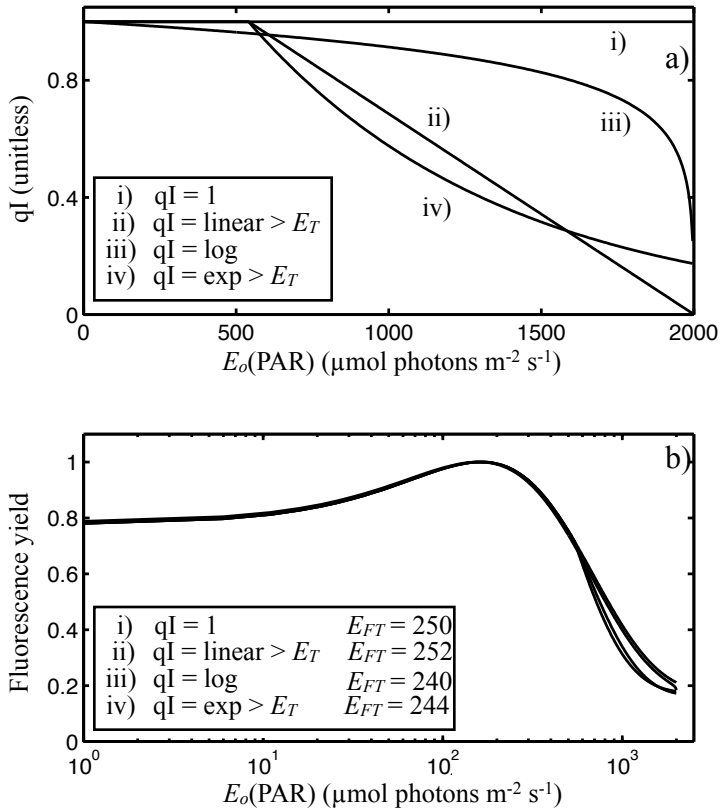

Figure a1. These two panels demonstrate the effects of varying qI as a function of irradiance on E_{FT}. Relative fluorescence yield was obtained from Eq. (4), a modified version of the Morrison (2003) model scaled to 1 (E_k = 150 µmol photons m^{-2} s^{-1}, E_T = 500 µmol photons m^{-2} s^{-1}, ϕ_{fo} = 0.04, $\phi_{f\max}$ = 0.09). The units for E_{FT} are (µmol photons m^{-2} s^{-1}).

A.3 Estimating Mean Mixed Layer Chlorophyll *a* Concentration

The SeaHorse™ data set has a unique time series of fluorescence profiles however, it is necessary to perform local calibrations with discrete chlorophyll *a* measurements to interpret these profiles as Chl*a*. A regression analysis between F' and measured extracted Chl*a* from 38 discrete chlorophyll *a* samples taken at night provided a local empirical relationship which was used to convert F' into estimates of chlorophyll *a* concentration (Fig. a2; Eq. a2):

$$\text{Chl}a = F' \cdot (0.80) - 1.1 \qquad \text{(a2)}$$

where 0.80 is the slope of the curve with units (mg Chl*a* m^{-3} rfu^{-1}), and -1.1 is the y-intercept (mg Chl*a* m^{-3}). This empirical relationship had a coefficient of determination of 0.83. Such a large coefficient of determination normally suggests that F' predicts a large amount of the variability observed in Chl*a*. In this case the large coefficient of determination is due to the large range of data, since there is scatter and missing data in the middle range of the data.

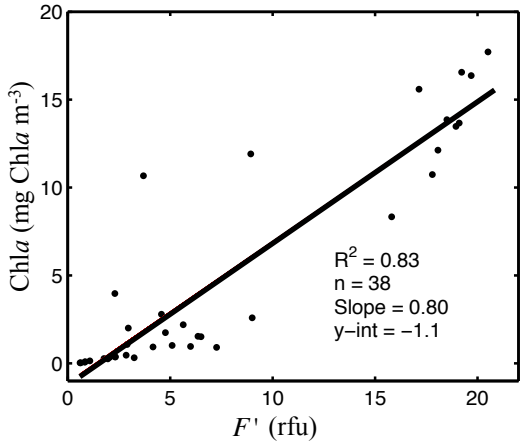

Figure a2. Measured Chl*a* taken from water samples near the location of the SeaHorse™ were compared with F' measured from the Seahorse™. Both Chl*a* and F' are positively correlated with a coefficient of determination of 0.83. All Chl*a* samples were obtained at night. Note this relationship is specific to the fluorometer used and the environment sampled.

Since the data used to obtain the parameters of Eq. (a2) were obtained at night, the relationship should only be applied to fluorescence profiles obtained at night. Therefore, the mean Chl*a* of the mixed layer ($\overline{Chl_\ell}$) was only determined from nighttime profiles. In order to assess whether or not $\overline{Chl_\ell}$, obtained from nighttime profiles is representative of the mean Chl*a* of the mixed layer during the day, the relationship between $\overline{Chl_\ell}$ and the diffuse downwelling attenuation coefficient determined from near surface to the base of the mixed layer ($K_d(\ell,443)$,

m^{-1}), was examined (Fig. a3). $K_d(\ell,443)$ was chosen because it can be measured during the day, and has been correlated with Chl*a* (Morel, 1988). The wavelength 443 nm was chosen since it is near the maximum spectral absorption coefficient of phytoplankton (Bricaud *et al.*, 1995). The relationship between $\overline{Chl_\ell}$ measured at night, and $K_d(\ell,443)$ measured the day after, yielded a relatively strong significant correlation ($p < 0.01$, $R^2 = 0.91$, $n = 18$), which provides evidence that $\overline{Chl_\ell}$ measured at night is a reasonable measure of the mean mixed layer Chl*a* during the day.

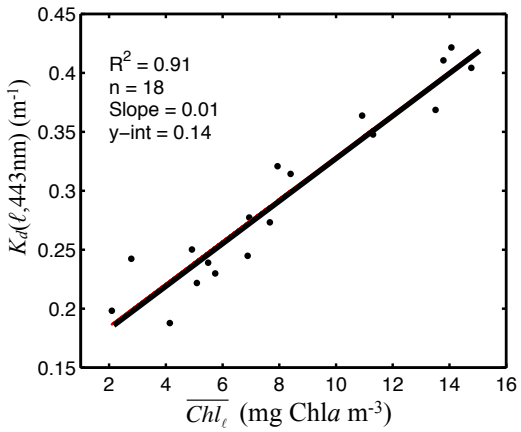

Figure a3. The correlation between the mean mixed layer diffuse downwelling attenuation coefficient (K_d(ℓ,443)) and the estimated mean chlorophyll *a* concentration of the mixed layer ($\overline{Chl_\ell}$), obtained from the SeaHorse™. Note, $\overline{Chl_\ell}$ estimates were obtained at night, and K_d(ℓ,443) estimates were obtained during the day.

A.4. Some Details About the E.F.T. Model

The parameter E_{FT} was determined by fitting the E.F.T. model to an *F vs. E* curve and optimizing its parameters. The optimization seeks to minimize the cost function, defined in this thesis as the sum of squares of the residuals between data and model. From an initial set of parameters, the optimization routine iteratively varies the parameters of the model to follow the steepest gradient of the cost function, leading to a minimum, i.e., the optimized parameter

estimate. Ideally the two-dimensional cost function will have a bowl shape (Fig. a4 a), when the gradient of the cost function will lead to a global minimum. However, the cost function can also appear as a trough (Fig. a4 b). In this case, changes in one parameter affect the cost function, but changes in the other do not. When a trough occurs it is difficult to obtain an optimal estimate of the particular parameter (parameter 2; Fig. a4 b), and the resulting error of the parameter is large.

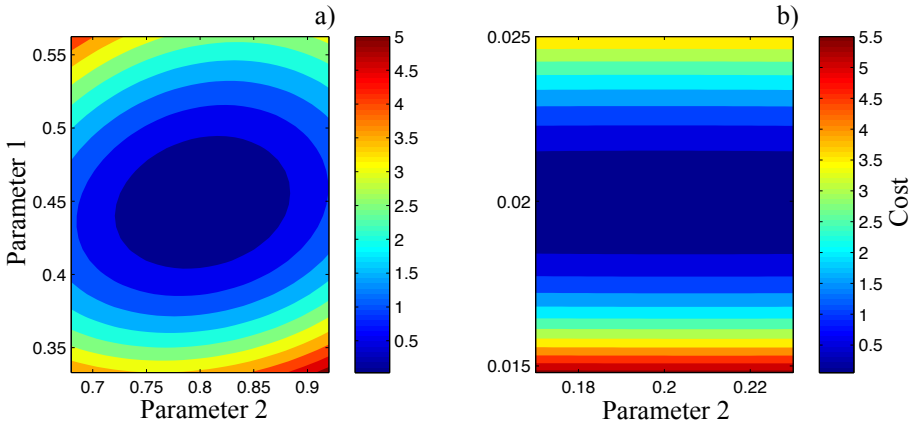

Figure a4. Examples of the two-dimensional cost functions: the 'bowl' shape (panel a), and the 'trough' shape (panel b).

The cost function of the E.F.T. model was examined with an artificial data set. The data set was generated using the E.F.T. model with a set of typical parameters (Table a1). By fitting the E.F.T. model to this artificial data set, but varying two of the four parameters at a time, the resulting two-dimensional cost function can be visualized. The two-dimensional cost function for all possible combination of parameters were examined (data not shown), and all exhibited a trough shape (such as the one in Fig. a4 b), except the two-dimensional cost function corresponding to the parameters F'_{EFT}, and m_1, which exhibited a shape somewhere between a trough and a bowl.

The Hessian matrix, the second order partial derivative of the cost function, can be used to examine aspects of the optimization. The condition number, which is the ratio of the highest

and lowest eigenvalue of the Hessian matrix is a measure of the shape of the cost function. When the condition number is large, the matrix is nearly singular, and the rate of convergence to the global minima is small, i.e., it is difficult to determine a unique parameter set. When the condition number is small, the rate of convergence of the optimization algorithm is large, and the resulting parameter estimates are more robust. The condition number of the artificial dataset mentioned above was high (10^7). One reason for obtaining high condition numbers could be if the order of magnitude for each parameter differs. The parameters of the E.F.T. model differed by 4 orders of magnitude (Table a1). Since the parameter E_{FT} is directly dependent of the units of the dependent variable of the E.F.T. model (E_o(PAR)), simply scaling the units of E_o(PAR) will change the order of magnitude of E_{FT}. By changing the units of E_o(PAR) from µmol photons m^{-2} s^{-1} to mmol photons m^{-2} s^{-1}, E_{FT} was reduced by three orders of magnitude. The resulting condition number was reduced to a more acceptable value of 134.

Table a1. Typical values of the E.F.T. model parameters determined from an average over all the data sets used in this thesis.

	E_o(PAR) (µmol photons m^{-2} s^{-1})	E_o(PAR) (mmol photons m^{-2} s^{-1})
F_{EFT}	0.9 rfu	0.9 rfu
E_{FT}	200 µmol photons m^{-2} s^{-1}	0.2 mmol photons m^{-2} s^{-1}
m_1	0.02 rfu	0.02 rfu
m_2	-0.4 rfu	-0.4 rfu

The eigenvectors belonging to the smallest eigenvalues of the Hessian matrix can provide information on parameter resolution (Fennel *et al.,* 2001). High values of eigenvectors can provide information on whether or not combinations of parameters can be determined or if they have large uncertainties. The eigenvector corresponding to the smallest eigenvalue from the

artificial data (Fig. a5 a) suggest that the parameters F'_{EFT}, E_{FT} and m_1, either have large uncertainty or that they covary in some way. The smallest eigenvector corresponds to the parameter m_2. This parameter describes the second slope of the E.F.T. model. The manner in which the E.F.T. model is formulated, a large proportion of data (>80%) is fit to the part of the curve that is described by the m_2 parameter (shaded region of Fig. a5 b), and could be the reason for the low eigenvector of m_2.

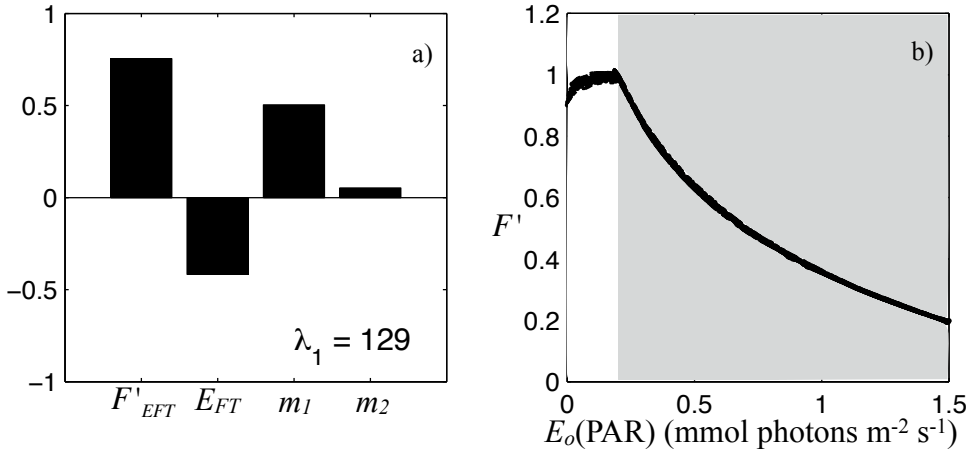

Figure a5. Panel a) Parameter resolution of the E.F.T. model using the artificial data set. Only the eigenvector corresponding to the smallest eigenvalue is provided. Panel b) The artificial data set generated by average parameter values (Table a1). The shaded region is described by the parameter m_2, and represents more than 80% of the data.

References

Adir, N., H. Zer, S. Shochat, and I. Ohad. 2003. Photoinhibition - a historical perspective. Photosynthesis Research **76:** 343-370.

Antoine, D., and A. Morel. 1996. Oceanic primary production, 1, Adaptation of a spectral light-photosynthesis model in view of application to satellite chlorophyll observations. Global Biogeochemical Cycles **10:** 43-55.

Babin, M., A. Morel, and B. Gentili. 1996a. Remote sensing of sea surface sun-induced chlorophyll fluorescence: consequences of natural variations in the optical characteristics of phytoplankton and the quantum yield of chlorophyll *a* fluorescence. International Journal of Remote Sensing **17:** 2417-2448.

Babin, M., A. Morel, H. Claustre, A. Bricaud, Z. Kolber, and P. G. Falkowski. 1996b. Nitrogen- and irradiance-dependent variations of the maximum quantum yield of carbon fixation in eutrophic, mesotrophic and oligotrophic marine systems. Deep Sea Research Part I: Oceanographic Research Papers **43:** 1241-1272.

Babin, M. 2008. Phytoplankton fluorescence: theory, current literature and *in situ* measurement, p. 237-280. *In* M. Babin, C. S. Roesler and J. J. Cullen [eds.], Real-time Coastal Observing Systems for Marine Ecosystem Dynamics and Harmful Algal Blooms. United Nations educational, Scientific and Cultural Organization.

Balch, W., R. Evans, J. Brown, G. Feldman, C. Mcclain, and W. Esaias. 1992. The remote sensing of ocean primary productivity: use of a new data compilation to test satellite algorithms. Journal of Geophysical Research **97:** 2279-2293.

Barber, R., and A. Hilting. 2002. History of the study of plankton productivity, p. 16-43. *In* P. J. le B. Williams, D. N. Thomas and C. S. Reynolds [eds.], Phytoplankton Productivity: Carbon assimilation in marine and freshwater ecosystems. Blackwell Science.

Barnett, A. 2005. Nonphotochemical quenching of fluorescence as a diagnostic of light history and nutrient stress in the diatom *Thalassiosira pseudonana*. MSc, Oceanography Department, Dalhousie University.

Behrenfeld, M. J., and P. G. Falkowski. 1997. Photosynthetic rates derived from satellite-based chlorophyll concentration. Limnology and Oceanography **42:** 1-20.

Behrenfeld, M. J. and others 2009. Satellite-detected fluorescence reveals global physiology of ocean phytoplankton. Biogeosciences **6:** 770-794.

Bishop, J., and W. B. Rossow. 1991. Spatial and temporal variability of global surface solar irradiance. Journal of Geophysical Research **96:** 16839-16858.

Boss, E. and others 2008. Observations of pigment and particle distributions in the western North Atlantic from an autonomous float and ocean color satellite. Limnology Oceanography **53:** 2112-2122.

Brainerd, K. E., and M. C. Gregg. 1995. Surface mixed and mixing layer depths. Deep-Sea Research Part I **42:** 1521-1543.

Bricaud, A., M. Babin, A. Morel, and H. Claustre. 1995. Variability in the chlorophyll-specific absorption coefficients of natural phytoplankton - analysis and parameterization. Journal of Geophysical Research-Oceans **100:** 13321-13332.

Campbell, J. and others 2002. Comparison of algorithms for estimating ocean primary production from surface chlorophyll, temperature, and irradiance. Global Biogeochemical Cycles **16:** 10.1029.

Carr, M. E. and others 2006. A comparison of global estimates of marine primary production from ocean color. Deep-Sea Research Part II **53:** 741-770.

Comeau, A. J. and others 2007. Monitoring the spring bloom in an ice covered fjord with the Land/Ocean Biogeochemical Observatory (LOBO). MTS/IEEE Oceans 2007, Sept 29 - Oct 4, Vancouver, BC.

Côté, B., and T. Platt. 1983. Day-to-day variations in the spring-summer photosynthetic parameters of coastal marine-phytoplankton. Limnology and Oceanography **28:** 320-344.

Cullen, J.J., and E. H. Renger. 1979. Continuous measurement of the DCMU-induced fluorescence response of natural phytoplankton populations. Marine Biology **53:**13-20.

Cullen, J. J. 1982. The deep chlorophyll maximum: comparing vertical profiles of chlorophyll *a*. Canadian Journal of Fisheries and Aquatic Sciences **39:** 791-803

Cullen, J. J., and F. M. H. Reid, and E. Stewart. 1982. Phytoplankton in the surface and chlorophyll maximum off southern California in August, 1978. Journal of Plankton Research **4:** 665-694

Cullen, J. J., and M. R. Lewis. 1988. The kinetics of algal photoadaptation in the context of vertical mixing. Journal of Plankton Research **10:** 1039.

Cullen, J. J., M. R. Lewis, C. O. Davis, and R. T. Barber. 1992a. Photosynthetic characteristics and estimated growth rates indicate grazing is the proximate control of primary production in the equatorial Pacific. Journal of Geophysical Research-Oceans **97:** 639-654.

Cullen, J. J., X. Yang, and H. L. MacIntyre. 1992b. Nutrient limitation of marine photosynthesis, p. 69-88. *In* P. Falkowski, G. and A. Woodhead, D. [eds.], Primary Productivity and Biogeochemical Cycles in the Sea. Plenum Press.

Cullen, J., and M. Lewis, R. 1995. Biological processes and optical measurements near the sea surface: Some issues relevant to remote sensing. Journal of Geophysical Research **100:** 13255-213266.

Cullen, J., A. Ciotti, R. Davis, and P. Neale. 1997. The relationship between near-surface chlorophyll and solar-stimulated fluorescence: biological effects. SPIE **2963:** 272-277.

Demers, S., S. Roy, R. Gagnon, and C. Vignault. 1991. Rapid light-induced changes in cell fluorescence and in xanthophyll-cycle pigments of *Alexandrium excavatum* (Dinophyceae) and *Thalassiosira pseudonana* (Bacillariophyceae): a photo-protection mechanism. Marine Ecology Progress Series **76:** 185-193.

Demmig-Adams, B., and W. W. Adams III. 1996. The role of xanthophyll cycle carotenoids in the protection of photosynthesis. Trends in Plant Science **1:** 21-26.

Denman, K. L., and A. E. Gargett. 1983. Time and space scales of vertical mixing and advection of phytoplankton in the upper ocean. Limnology and Oceanography **28:** 801-815.

Eppley, R. W., and B. J. Peterson. 1979. Particulate organic matter flux and planktonic new production in the deep ocean. Nature **282:** 677-680.

Falkowski, P., and D. A. Kiefer. 1985. Chlorophyll-*a* fluorescence in phytoplankton - relationship to photosynthesis and biomass. Journal of Plankton Research **7:** 715-731.

Falkowski, P., and J. A. Raven. 1997. Aquatic Photosynthesis. First ed. Blackwell Science.

Fennel, K., M. Losch, J. Schröter, and M. Wenzel. 2001. Testing a marine ecosystem model: sensitivity analysis and parameter optimization. Journal of Marine Systems **28:** 45-63.

Flemer D. A. 1969. Continuous measurement of *in vivo* chlorophyll of dinoflagellate bloom in Chesapeake Bay. Chesapeake Science **10:** 99-103

Goebel, N. L., and J. N. Kremer. 2007. Temporal and spatial variability of photosynthetic parameters and community respiration in Long Island Sound. Marine Ecology Progress Series **329:** 23-42.

Gordon, H. R., D. K. Clark, J. L. Mueller, and W. A. Hovis. 1980. Phytoplankton pigments from the Nimbus-7 Coastal Zone Color Scanner: comparisons with surface measurements. Science **210:** 63-66.

Guillard, R. R. L., and P. E. Hargraves. 1993. *Stichochrysis immobilis* is a diatom, not a chrysophyte. Phycologia **32:** 234-236.

Hamilton, J. M., G. A. Fowler, and B. D. Beanlands. 1999. Long-term monitoring with a moored wave-powered profiler. Sea Technology **40:** 68-69.

Harding, L. W., B. B. Prezelin, B. M. Sweeney, and J. L. Cox. 1982. Diel oscillations of the photosynthesis-irradiance (PI) relationship in natural assemblages of phytoplankton. Marine Biology **67:** 167-178.

Harrison, W. G., and T. Platt. 1986. Photosynthesis-irradiance relationships in polar and temperate phytoplankton populations. Polar biology **5:** 153-164.

Herzig, R., and P. G. Falkowski. 1989. Nitrogen limitation in *Isochrysis galbana*(Haptophyceae). 1. Photosynthetic energy conversion and growth efficiencies. Journal of Phycology **25:** 462-471.

Holm-Hansen, O., A. F. Amos, and C. D. Hewes. 2000. Reliability of estimating chlorophyll *a* concentrations in Antarctic waters by measurement of *in situ* chlorophyll *a* fluorescence. Marine Ecology Progress Series **196:** 103-110.

Horton, P., A. V. Ruban, and R. G. Walters. 1996. Regulation of light harvesting in green plants. Annual Review of Plant Physiology and Plant Molecular Biology **47:** 655-684.

Iverson, R. L. 1990. Control of marine fish production. Limnology and Oceanography **35:** 1593-1604.

Jannasch H. W.m L. J. Coletti, K. S. Johnson, S. E. Fitzwater, J. A. Needoba, J. N. Plant. 2008. The Land/Ocean Biogeochemical Observatory: a robust networked mooring system for continuously monitoring complex biogeochemical cycles in estuaries, Limnology and Oceanography: Methods **6**: 263-276.

Jassby, A. D., and T. Platt. 1976. Mathematical formulation of the relationship between photosynthesis and light for phytoplankton. Limnology and Oceanography **21:** 540-547.

Jerome, J. H., R. P. Bukata, and J. E. Bruton. 1988. Utilizing the components of vector irradiance to estimate the scalar irradiance in natural waters. Applied Optics **27:** 4012-4018.

Johnson, Z. I. 2004. Description and application of the background irradiance gradient-single turnover fluorometer (BIG-STf). Marine Ecology Progress Series **283:** 73-80.

Kiefer, D. A. 1973. Fluorescence properties of natural phytoplankton populations. Marine Biology **22:** 263 - 269.

Kiefer, D. A., and R. A. Reynolds. 1992. Advances in understanding phytoplankton fluorescence and photosynthesis, p. 155-174. *In* P. Falkowski and A. Woodhead, D. [eds.], Primary Productivity and Biogeochemical Cycles in the Sea. Plenum Press.

Kirk, J. 1994. Light & Photosynthesis in Aquatic Ecosystems, Second ed. Cambridge University Press.

Koblentz-Mishke, O. J., V. V. Volkovinsky, and J. G. Kabanova. 1970. Plankton primary production of the World Ocean. 183-193. Scientific Exploration of the South Pacific. W.S. Wooster.

Kolber, Z., and P. G. Falkowski. 1993. Use of active fluorescence to estimate phytoplankton photosynthesis *in-situ*. Limnology and Oceanography **38:** 1646-1665.

Krause, G. H., and E. Weis. 1991. Chlorophyll fluorescence and photosynthesis: the basics. Annual Review of Plant Biology **42:** 313-349.

Krupatkina, D. K., Z. Z. Finenko, and A. A. Shalapyonok. 1991. Primary production and size-fractionated structure of the black-sea phytoplankton in the winter-spring period. Marine Ecology-Progress Series **73:** 25-31.

Kyewalyanga, M. N., T. Platt, S. Sathyendranath, V. A. Lutz, and V. Stuart. 1998. Seasonal variations in physiological parameters of phytoplankton across the north Atlantic. Journal of Plankton Research **20:** 17-42.

Laney, S. R., R. M. Letelier, and M. R. Abbott. 2005. Parameterizing the natural fluorescence kinetics of *Thalassiosira weissflogii*. Limnology and Oceanography **50:** 1499-1510.

Letelier, R. M., M. R. Abbott, and D. M. Karl. 1997. Chlorophyll natural fluorescence response to upwelling events in the Southern Ocean. Geophysical Research Letters **24:** 409-412.

Lewis, M. R., and J. C. Smith. 1983. A small volume, short-incubation-time method for measurement of photosynthesis as a function of incident irradiance. Marine Ecology Progress Series **13**: 99-102.

Lewis, M. R., J. J. Cullen, and T. Platt. 1984. Relationships between vertical mixing and photoadaptation of phytoplankton - similarity criteria. Marine Ecology Progress Series **15:** 141-149.

Loftus, M. E., and H. Seliger. 1975. Some limitations of the *in vivo* fluorescence technique. Chesapeake Science **16:** 79-92.

Loisel, H., and A. Morel. 1998. Light scattering and chlorophyll concentration in case 1 waters: a reexamination. Limnology and Oceanography **43:** 847-858.

Longhurst, A., S. Sathyendranath, T. Platt, and C. Caverhill. 1995. An estimate of global primary production in the ocean from satellite radiometer data. Journal of Plankton Research **17:** 1245-1271.

Lorenzen, C. J. 1966. A method for the continuous measurement of *in vivo* chlorophyll concentration. Deep-Sea Research **13:** 223-227.

MacIntyre, H. L., T. M. Kana, T. Anning, and R. J. Geider. 2002. Photoacclimation of photosynthesis irradiance response curves and photosynthetic pigments in microalgae and cyanobacteria. Journal of Phycology **38:** 17-38.

Marshall, S. M., and A. P. Orr. 1928. The photosynthesis of diatom cultures in the sea. Journal of the Marine Biological Association of the United Kingdom **15:** 321-360.

Morel, A. 1988. Optical modeling of the upper ocean in relation to its biogenous matter content (case I waters). Journal of Geophysical Research **93:** 749-768.

Morrison, J. R. 2003. In situ determination of the quantum yield of phytoplankton chlorophyll *a* fluorescence: a simple algorithm, observations, and a model. Limnology and Oceanography **48:** 618-631.

Morrison, J. R., and D. S. Goodwin. 2010. Phytoplankton photocompensation from space-based fluorescence measurements. Geophysical Research Letters **37**, **doi:10.1029/2009GL041799**.

Neale, P. J., and P. J. Richerson. 1987. Photoinhibition and the diurnal variation of phytoplankton photosynthesis-I. Development of a photosynthesis-irradiance model from studies of *in situ* responses. Journal of Plankton Research **9:** 167-193.

Neale, P. J., J. J. Cullen, and C. M. Yentsch. 1989. Bio-optical inferences from chlorophyll *a* fluorescence: what kind of fluorescence is measured in flow cytometry? Limnology and Oceanography **34:** 1739-1748.

Niewiadomska, K., H. Claustre, L. Prieur, and F. d'Ortenzio. 2008. Submesoscale physical-biogeochemical coupling across the Ligurian Current (northwestern Mediterranean) using a bio-optical glider. Limnology and Oceanography **53:** 2210-2225.

Oliver, R. L., J. Whittington, Z. Lorenz, and I. T. Webster. 2003. The influence of vertical mixing on the photoinhibition of variable chlorophyll *a* fluorescence and its inclusion in a model of phytoplankton photosynthesis. Journal of Plankton Research **25:** 1107:1129.

Parkhill, J.-P., G. Maillet, and J. J. Cullen. 2001. Fluorescence-based maximal quantum yield for PSII as a diagnostic of nutrient stress. Journal of Phycology **37:** 517-529.

Parkhill, J.-P. 2003. Fluorescence as a diagnostic of nutrient stress. PhD, Oceanography Dept., Dalhousie University.

Perry, M. J., B. S. Sackmann, C. C. Eriksen, and C. M. Lee. 2008. Seaglider observations of blooms and subsurface chlorophyll maxima off the Washington coast. Limnology and Oceanography **53**: 2169-2179.

Petrie, B. 2004. The Halifax Section : A Brief History. AZMP Bulletin **4**: 26-29.

Platt, T., C. L. Gallegos, and W. G. Harrison. 1980. Photoinhibition of photosynthesis in natural assemblages of marine phytoplankton. Journal of Marine Research **38:** 687-701.

Platt, T. 1986. Primary production of the ocean water column as a function of surface light-intensity - algorithms for remote-sensing. Deep-Sea Research Part a-Oceanographic Research Papers **33:** 149-163.

Platt, T., S. Sathyendranath, C. M. Caverhill, and M. R. Lewis. 1988. Ocean primary production and available light - further algorithms for remote-sensing. Deep-Sea Research Part a-Oceanographic Research Papers **35:** 855-879.

Platt, T., S. Sathyendranath, and P. Ravindran. 1990. Primary production by phytoplankton: analytic solutions for daily rates per unit area of water surface. Proceedings: Biological Sciences **241:** 101-111.

Platt, T., and S. Sathyendranath. 1993. Estimators of primary production for interpretation of remotely-sensed data on ocean color. Journal of Geophysical Research-Oceans **98:** 14561-14576.

Platt, T. and others. 2008. Operational estimation of primary production at large geographical scales. Remote Sensing of Environment **doi:10.1016/j.rse.2007.11.018**.

Prézelin, B. B., and H. A. Matlick. 1980. Time-course of photoadaptation in the photosynthesis-irradiance relationship of a dinoflagellate exhibiting photosynthetic periodicity. Marine Biology **58:** 85-96.

Ragni, M., R. L. Airs, N. Leonardos, and R. J. Geider. 2008. Photoinhibition of PSII in *Emiliania huxleyi* (Haptophyta) under high light stress: the roles of photoacclimation, photoprotection, and photorepair. Journal of Phycology **44:** 670-683.

Sackmann, B. S., M. J. Perry, and C. C. Eriksen. 2008. Seaglider observations of variability in daytime fluorescence quenching of chlorophyll-*a* in Northeastern Pacific coastal waters. Biogeosciences Discuss **5:** 2839-2865.

Sakshaug, E., S. Demers, and C. M. Yentsch. 1987. *Thalassiosira oceanica* and *T. pseudonana*: two different photoadaptational responses. Marine Ecology Progress Series **41:** 275-282.

Sakshaug, E. and others 1997. Parameters of photosynthesis: definitions, theory and interpretations of results. Journal of Plankton Research **19:** 1637-1670.

Sathyendranath, S., and T. Platt. 1989. Computation of aquatic primary production: extended formalism to include effect of angular and spectral distribution of light. Limnology and Oceanography **34**: 188-198.

Schallenberg, C., M. R. Lewis, D. E. Kelley, and J. J. Cullen. 2008. Inferred influence of nutrient availability on the relationship between sun-induced chlorophyll fluorescence and incident irradiance in the Bering Sea. Journal of Geophysical Research-Oceans **113,** C07046, **doi: 10.1029/2007JC004355**.

Schreiber, U., H. Hormann, C. Neubauer, and C. Klughammer. 1995. Assessment of photosystem II photochemical quantum yield by chlorophyll fluorescence quenching analysis. Australian Journal of Plant Physiology **22:** 209-220.

Shaw, P. J., and D. A. Purdie. 2001. Phytoplankton photosynthesis-irradiance parameters in the near-shore UK coastal waters of the North Sea: temporal variation and environmental control. Marine Ecology Progress Series **216:** 83-94.

Stramski, D., and R. A. Reynolds. 1993. Diel variations in the optical properties of a marine diatom. Limnology and Oceanography **38:** 1347-1364.

Swertz, O. C., F. Colijn, H. W. Hofstraat, and B. A. Althuis. 1999. Temperature, salinity, and fluorescence in southern North Sea: high-resolution data sampled from a ferry. Environmental management **23:** 527-538.

Talling, J. F. 1957. Photosynthetic characteristics of some freshwater plankton diatoms in relation to underwater radiation. New Phytologist **56:** 29-50.

Vincent, W. 1983. Phytoplankton production and winter mixing: contrasting effects in two oligotrophic lakes. Journal of Ecology **71:** 1-20.

Vincent, W., P. Neale, and P. Richerson. 1984. Photoinhibition: algal responses to bright light during diel stratification and mixing in a tropical alpine lake. Journal of Phycology **20:** 201-211.